78-1458

Application of Hypersonic Favorable Aerodynamic Interference Concepts to Supersonic Aircraft

R. M. Kulfan,
Boeing Commercial Airplane Co., Seattle, Wash.

AIAA AIRCRAFT SYSTEMS AND TECHNOLOGY CONFERENCE

Los Angeles, Calif./August 21-23, 1978

APPLICATION OF HYPERSONIC FAVORABLE AERODYNAMIC INTERFERENCE CONCEPTS TO SUPERSONIC AIRCRAFT

R.M. Kulfan, Senior Specialist Engineer
Boeing Commercial Airplane Company, Seattle, Washington

Abstract

A study was made to identify hypersonic favorable aerodynamic interference concepts for application to supersonic aircraft. Preliminary aerodynamic analysis defined key design parameters, and scoped potential aerodynamic efficiency improvements. The study included supersonic biplanes, ring wings, parasol wings, wave rider concepts, and flat-top wing/body arrangements. Results indicate the parasol wing concept offers the greatest potential aerodynamic benefits for the study conditions. However, the best aerodynamic concept is very dependent on the design Mach number, and on the airplane component size relationships. It is shown that existing aerodynamic design/analysis methods can be used for parasol wing aerodynamics studies.

1.0 Introduction

Aircraft capable of extended range while cruising at supersonic Mach numbers are of interest for both commercial[1] and military applications[2]. Existing supersonic airplanes and current study configurations typically employ thin, highly swept wings and slender bodies that are integrated with the propulsion system and other components to produce aerodynamically efficient designs. Through careful design, these configurations can derive favorable aerodynamic interference effects associated with mutual interactions of the flow fields created by airplane components. The interactions can result in direct drag reduction, or in additional lift production. Body area ruling[3] and wing mounted engine installations[4] are well-known examples.

Enhancing favorable aerodynamic interference effects offers the potential for further increases in supersonic aerodynamic efficiency. Considerable development of favorable interference technology took place in studies of maneuverable orbital entry vehicles and hypersonic vehicles. Application of these favorable aerodynamic interference concepts to supersonic aircraft has not been explored in depth.

A study[5] was made to evaluate potential aerodynamic benefits of using these hypersonic concepts for supersonic aircraft. The aerodynammic design results of this study form the subject of this paper.

The aerodynamic design/analysis methods that were used in the study are summarized in Section 2.0. This section is followed by a review of the general aerodynamic design criteria applied to the study configurations, Section 3.0. This section also contains a review of the different aerodynamic features of aircraft designed for subsonic flight, for supersonic flight, or for hypersonic flight. Hypersonic and favorable interference concepts selected for this study are also identified.

Sections 4.0 through 7.0 contain results of evaluations of the various aerodynamic concepts considered in this study. These sections also summarize the physics of the aerodynamics of each concept.

The parasol wing was identified as the most promising concept. Section 8.0 contains aerodynamic design guidelines for parasol wing configurations. The parasol wing configuration developed in this study is described and evaluated in Section 9.0.

The main aerodynamic conclusions of the study are summarized in Section 10.0.

2.0 Theoretical Aerodynamic Methods

Aerodynamic design and analysis methods that were used in the study are described in this section. The particular methods used for a specific aerodynamic concept depended on the nature of the configuration, and on the desire to use the most efficient applicable analytical tool. Throughout the study, slender body theory estimates provided design guidance, and also identified significant design parameters.

Exact shock expansion techniques were used to evaluate the supersonic aerodynamic characteristics of the nonplanar caret wing and Nonweiler wing concepts described in Section 5.0.

The aerodynamic design and analysis system for supersonic aircraft[6] (ADASSA) and the FLEXSTAB system[7] were used for design and analysis of the reference configurations and the parasol wing configurations (Sections 8.0 and 9.0).

ADASSA is currently one of the best supersonic design and analysis tools. This code is restricted to planar wings, where the lifting surfaces lie in a single plane. The code does include nonlinear methods for calculating shock waves produced by general bodies of revolution, and for determining the intersection of the shock waves and pressure fields with adjacent wings and bodies.

The aerodynamic influence coefficient (AIC) method used in FLEXSTAB provides the design and analysis capability for supersonic as well as subsonic planar or nonplanar aerodynamic configurations.

Both of these methods are small-disturbance potential flow methods, and are, therefore, restricted to slender-body, thin-wing arrangements producing weak shock waves. It is shown in Section 8.0 that both methods can predict the aerodynamic characteristics of parasol wing configurations.

3.0 Aerodynamic Concepts

The operating efficiency of an airplane is related to its ability to produce lift at low drag levels. Hence, the aerodynamic design goal is to shape and arrange components of the airplane to minimize the drag and/or to enhance the lift production. It seems possible that, in supersonic flight, unconventional arrangements of wings and bodies may offer advantages of drag reductions at cruise. It is desired to determine if any unconventional arrangement of wings and bodies offers sufficient advantage in the form of supersonic drag reduction to merit more detailed study.

Classes of airplanes can be defined according to the types of flow associated with the airplane[8,9]. Aircraft shapes that achieve a specific type of flow can then be readily identified or conceived. This approach was useful in identifying fundamental aerodynamic characteristics of the study configurations.

Acceptable aircraft designs must meet certain aerodynamic design criteria. These criteria include these factors:

- The airplane must be capable of achieving acceptable aerodynamic performance
- The flow must be physically achievable
- The flow over the aircraft must be stable and controllable
- The aircraft must be capable of flying at low speed to meet takeoff and landing requirements
- The airplane must be controllable

3.1 Types of Aircraft

Four types of aircraft are identified in Figures 1 and 2. The classical and swept wing aircraft are quite similar. In fact, the swept wing aircraft is an extension to higher speeds of the classical aircraft concepts. The geometry of classical and swept wings can be described as being conical, with the apex of the cone at the wing tip[10]. Span wise pressure changes on the classical wings are much smaller than the chordwise pressure changes. The flow over these wings is nearly two-dimensional in streamwise planes. The wings have sharp trailing edges, so that flow separation is confined and fixed to the trailing-edge area. It is possible to control this type of flow, and the associated forces and moments, to allow a sufficient range of practical flight conditions. The flow of these configurations is essentially subsonic. Means for providing volume, lift, thrust, and control are typically separate from each other.

The flow field for slender wings is also conical. In this case, the apex of the cone is at the wing apex. The streamwise pressure changes for very slender wings are milder than the spanwise pressure changes. The flow over these wings is effectively subsonic, except, perhaps, for localized areas near the wing trailing edge. The flow over these wings is attached for a rather limited angle of attack regime. A series of design criteria for achieving attached flow at supersonic speeds are discussed in Reference 11.

The most obvious aerodynamic characteristic of slender wings is the formation of rather stable leading-edge vortices at increased angle of attack. The angle of attack at which the flow separation and leading-edge vortices start depends on the airfoil leading-edge radius, and wing camber and twist[11]. The flow is attached on the wing behind the vortices, up to high incidence angles. When the leading-edge vortices develop, the drag due to lift increases because of loss of leading-edge suction[11]. The lift and pitching moment continue to increase. The components of the airplane that provide lift, volume, and thrust again tend to be separate. However, the components are carefully tailored to maximize aerodynamic efficiency through mild favorable interference effects[3].

The final class of aircraft, and the one of particular interest for this study, is the wave producer family. This family, as mentioned in Section 1.0, has been studied in conjunction with hypersonic configurations. The wave producer family differs from the previously mentioned types of aircraft in the following principal areas:

- Flow over the configuration is fundamentally supersonic at cruise. Shock waves and expansion waves in the stream are a predominant feature of the flow, and cannot be avoided. The shock waves are used to produce compression lift. The shock waves and expansion waves can interact to produce drag reductions.
- At lower speed, the flow changes to a subsonic type of flow similar to the slender wing. The change in flow is gradual and controllable.

Aircraft of the wave producer family tend to be highly integrated. In some concepts, the volume, lift, and thrust producing components are aerodynamically indistinguishable.

A convenient way to characterize the aerodynamics and geometry of the various types of aircraft is by the slenderness ratio, s/l. This is the ratio of the wing semispan to overall airplane length. The application regimes of these aircraft are shown in Figure 2. The different flow regimes for a wave producer configuration are also shown.

Only the slender wings and wave producing concepts are acceptable for high supersonic cruise flight.

3.2 Supersonic Drag

The drag of a conventional airplane at supersonic speeds consists of four major drag items:

- Skin friction drag, C_{D_F}
- Vortex drag, as in subsonic flow, C_{D_V}
- Wave drag due to volume, C_{D_W}
- Wave drag due to lift, $C_{D_{WL}}$

Figure 3 shows the effect of the aircraft slenderness ratio on these drag components. As the Mach number is increased, the optimum aircraft becomes more slender, to compensate for increasing wave drag due to lift.

The low-speed lift capability of very slender wings is shown

in Figure 4, as the ratio of required wing area to the wing area associated with the lift of a two-dimensional classical type wing. The lift associated with the formation of the leading-edge vortices becomes important for slender wings. However, the wing area necessary to fly at low speeds increases rapidly as the configuration becomes more slender.

In general, the total wave drag of a supersonic configuration is large. Objectives of most favorable supersonic aerodynamic interference concepts are to produce direct reduction in wave drag, or indirect drag reduction by creating interference lift. Other drag items, such as friction drag or vortex drag, are not to be increased excessively.

When considering hypersonic types of configuration for supersonic applications, as in this study, it is important to note Mach number influences on various aerodynamic forces. As shown in Figure 5, compression lift becomes more important than expansion lift at high Mach numbers. Base pressure tends to decrease. Consequently, many hypersonic aircraft designs tend to produce compression lift and to have significant base areas. Design modifications would be required for lower supersonic speed applications.

3.3 Aerodynamic Concept Selections

The identification of candidate favorable aerodynamic interference concepts for consideration in this study was initiated by a literature survey of technical references that describe features and applications of various interference concepts. The literature search revealed a number of potentially applicable interference concepts, shown in Figure 6. Qualitative assessments were made to determine which of these concepts were most suitable for application to meet the mission and design objectives.

The caret wing, Nonweiler wing, supersonic biplane, and parasol wing concepts were then identified as the potentially most promising concepts. The study effort was then directed at obtaining a fundamental understanding of the desirable aerodynamic features of the selected concepts, and to better define the potential aerodynamic efficiency of configurations incorporating these concepts. Aerodynamics of the various concepts are discussed in the sections that follow.

A principal design Mach number of 3.0 was selected for the results presented in this paper. This selection eased the design integration tasks of incorporating the favorable aerodynamic interference concepts. This aerodynamic design task becomes more difficult at lower supersonic Mach numbers, because of the greater areas of the flow field affected by shock waves and expansion waves produced by the aircraft components. The configurations considered in this study were representative of a small supersonic cruise military type aircraft.

4.0 Supersonic Biplanes

The Busemann supersonic biplane offers the potential of significant reduction in wing thickness drag[12, 13, 14, 15]. The drag reductions, as shown in Figure 7, can be obtained by mutual thickness interference between two wing panels, and also by interference between the lifting pressures on one wing acting on the thickness on an adjacent wing panel. The Busemann biplane type of interference is commonly called wave cancellation, since the shock waves produced by one surface are cancelled by an expansion pressure field produced on an adjacent surface.

Adjacent reflection surfaces are necessary to achieve the drag reduction. The reflection surface increases the friction drag. The drag due to lift interference is typically unfavorable, since the drag due to lift of the biplane is higher than that of the isolated individual surfaces.

The wing thickness wave drag reductions must exceed increases in friction drag, and drag due to lift, to show any net cruise drag benefit. The net aerodynamic benefits of a supersonic biplane were considered typically small, and were not investigated further in the study.

5.0 Caret and Nonweiler Wings

Previous hypersonic studies[9, 16 through 20] have indicated that the caret wing and Nonweiler wing concepts offer higher aerodynamic efficiency potential at very high supersonic Mach numbers than do conventional slender wing configurations. The aerodynamic features of the caret wing and Nonweiler wing concepts are shown in Figure 8.

The caret wing is designed to produce the same flow field as an equivalent two-dimensional wedge having its top lined up with the free stream. In an inviscid flow, the wedge shock wave is attached to the leading edge, and is a plane surface below the wedge.

The upper surface of the caret wing is aligned with the free stream. The wing leading edge at the supersonic design condition lies on the equivalent wedge planar shock wave. The caret wing lower surface is formed by streamlines in the flow behind the shockwave that passes through the wing leading intersection. This results in a three-dimensional wing configuration with an open base, and has the undisturbed free stream pressure over its top surface. The pressure on the lower surface is uniform, and equal to the pressure behind the shock in two-dimensional wedge flow.

The Nonweiler wing is formed by addition of an interference wing to a caret wing. The interference wing increases lift without increasing the slope of the main wing.

It was shown in Section 3 that compression lift is more effective than upper surface suction lift at high supersonic Mach numbers. Additionally, it was shown that base drag tends to be small. Hence, the caret wing and Nonweiler wing concepts offer relatively high lift/drag (L/D) ratios at high supersonic speeds as shown in Figure 8.

Exact shock wave relations were used to calculate the effects of Mach number, wedge angle, and planform slenderness ratio, s/l, on the design lift/drag ratios of caret wings. The results are shown in Figure 9.

The optimum wedge angle of the caret wing is approximately 4 deg at Mach 3.0, and increases slightly with higher design Mach numbers. Wing slenderness ratios in the order of 0.3 to 0.5 result in lift/drag ratios near maximum. Hence, the optimum caret wing has a larger wing span than the optimum slender wings shown in Figure 3.

The anhedral angle of the caret wing depends on the wedge angle, slenderness ratio, and design Mach number of the caret wing. The large anhedral at lower Mach numbers probably restricts the usefulness of the caret wing to the higher supersonic Mach numbers.

Similar calculations indicate that the Nonweiler "W" wing, shown in Figure 8, produces higher lift/drag ratios than a caret wing. In addition, the required anhedral angles of the Nonweiler wing are less than for caret wings [18].

The lift/drag ratio was calculated for a configuration incorporating a Mach 3.0 Nonweiler "W" wing design. The body and wing planform used for this study are shown in Figure 10.

In order to identify the impact on lift/drag ratio of integrating the Nonweiler wing concept into an airplane configuration, the following analyses were made:

- Isolated Nonweiler wing with the upper surface aligned with the free stream and with zero base drag. The lift and drag are the forces associated with the lower surface compression pressures.
- The skin friction drag on the upper and lower surfaces was then included.
- The wing upper surface was then modified to close the airfoils at the trailing edge. Double wedge airfoil sections were selected. The wing thickness/chord ratio, and the chordwise location of the maximum thickness, were varied. These changes introduced upper surface suction lift and wave drag.
- The friction and wave drag of the fuselage and fins were added to obtain the total configuration lift/drag values.

Results indicate that integrating the Nonweiler wing into an airplane configuration reduced the $(L/D)_{MAX}$ potential from 18, for the basic isolated wing without closing, to approximately 6.4, for the complete airplane. The suction lift produced by closing the wing airfoils more than compensated for the upper surface pressure drag, and resulted in an increase in aerodynamic efficiency L/D at the higher lift coefficients. The location of the wing maximum thickness was found not to be important. Increased wing thickness and the drag of the body and fins have a significant effect on L/D.

The drag of the Nonweiler wing configuration was compared with the drag of a conventional type airplane. The L/D of the Nonweiler wing configuration is approximately equal to that of the optimized conventional airplane.

6.0 Flat-top Wing/Body Configuration

An alternative form of a wave rider concept is the flat-top wing/body arrangement[21 through 26]. The body area growth under the wing produces a bow shock, followed by a compression pressure field. The wing leading edge coincides with the bow shock at the design Mach number. The body pressures, as shown in Figure 11, fall upon the wing lower surface to produce an interference lift increment, ΔC_L. The interference lift depends on the body area growth and Mach number

$$\Delta C_L = \frac{2\, A_{BODY}}{\beta\, S_{REF}}$$

A_{BODY} = Body base area
S_{REF} = Reference wing area
$\beta = \sqrt{M^2-1}$
M = Mach number

The interference lift allows the configuration to fly at a lower angle of attack. This effect results in a reduction in drag due to lift.

The body wave drag of this configuration, however, is greater than the body wave drag of an equal area symmetric wing/body configuration. The wing lower surface pressures, when the wing is at an angle of attack, push on the forebody, producing an unfavorable wing-on-body interference. The unfavorable wing-on-body interference and the increase in body wave drag tend to cancel the favorable lift interference effects.

The lift produced by the flat-top wing/body combination can be increased by wing anhedral, as shown in Figure 12. The body wave drag for equal base areas is, however, also increased by wing anhedral. Additionally, wing anhedral reduces the wing lift curve slope.

The potential aerodynamic benefits of a flat-top wing/body concept with or without anhedral over a symmetric wing/body arrangement are, therefore, small for the present study design requirements.

Results of studies exploring the aerodynamic characteristics of ring wings and parasol wings are described in the next section.

7.0 Ring Wings and Parasol Wings

The ring-wing configuration (Figure 6) is a three-dimensional application of the Busemann biplane wave cancellation concept described in Section 4.0. The ring wing is designed to reflect forebody compression pressures back, to push on the aft end of the body. This effect can result in zero body wave drag.

The half-ring wing concept retains part of the body wave drag cancellation, but produces an interference lift associated with the forebody pressures glancing off the wing lower surface. This effect produces a more efficient lifting system.

The parasol wing concept is a further adaptation of the half-ring wing concept, designed to enhance the overall aerodynamic efficiency of the configuration.

Previous investigations[25, 27 through 41] have shown that

the parasol wing/body arrangement can combine wave-cancellation and interference lift effects into an aerodynamically efficient design. The body in a parasol wing arrangement is positioned below the wing, so that, at supersonic speeds, the bow shock and forebody pressure field impact on the wing lower surface. The body wave cancellation effect is produced by the body pressures glancing off the wing surface, and back onto the aft end of the body. This effect produces a thrusting force. The body pressures reflecting off the wing also produce a favorable interference lift force. The wing lower surface lifting pressures push on the aft end of the body to produce a favorable thrust force. The aerodynamic features of the parasol wing are shown in Figure 13.

Parametric studies were made to investigate body wave drag cancellation, and interference lift generation for a body located below a wing. The objective of these investigations was to scope aerodynamic benefits of configurations employing the parasol wing concept. The results are summarized in this section.

The wave drag calculations were made using the far-field wave drag calculation program of ADASSA. Image bodies, as shown in Figure 14, were used to represent various wing geometries. The wing geometry variations include wing anhedral, and simple rectangular shroud arrangements, to represent ring wings and half-ring wings.

The analyses were made for Mach 3.0. However, the results can be applied to other Mach numbers by scaling the spacing distances by the ratio $\sqrt{\frac{8}{M^2-1}}$.

The study focused on identifying the importance of body spacing, wing dihedral, and parasol curvature effects for enhancing the body wave drag cancellation.

The effects of wing dihedral and body spacing on body wave drag are shown in Figure 15. The effects of flat wing reflection, 45% dihedral wing, half-shroud wing, and full-shroud wing on body wave drag are shown in Figure 16. The optimum half-shroud arrangement reduced the body wave drag by nearly 50%.

Additional wave drag analyses were made of the simple rectangular half-shrouded wing arrangement. Shroud geometries having different ratios of shroud width, S_w, to shroud height, S_h, were investigated. For each arrangement, the shroud height was varied to determine the minimum drag arrangement. The optimum shroud geometries for the rectangular shroud are shown in Figure 17. These results indicate that for a design Mach number of 3.0, a low-drag shroud should have a semispan of 1.4 body diameters, and be located 1.2 diameters above the body centerline.

The body pressures acting on the reflection surfaces of the flat wing, dihedral wing, or half-shrouded wing also produce an interference lift. The amount of interference lift depends on the portion of body pressures captured by the wing surface.

Slender body theory was used to estimate the effects of wing anhedral on the interference lift. The effect of wing anhedral can be calculated by representing the wing and body geometry by the body plus an appropriate number of image bodies, as shown in Figure 18. The number of required images, N_i, can be related to the anhedral angle, Γ, by the relation:

$$Ni = \left(\frac{2}{1-\frac{\Gamma}{90}}\right) - 1$$

The body and every required image body contribute an equal amount to the pressure interference force, $(1/\beta \cdot A_{END}/S_{REF})$. The number of required images increases as the anhedral angle increases. This increases the interference pressure force, N, which is normal to the wing surface. Hence, only a portion of the increased interference pressure acts in the lift direction, $(L = N \cos \Gamma)$. The net results, as shown in Figure 18, indicate that the effect of anhedral angle on interference lift is exactly the same as predicted for the flat-top wing/body arrangement (Figure 12).

The parasol wing and flat-top wing/body concepts are, therefore, equally efficient in producing interference lift. The parasol wing, however, by virtue of the wave cancellation effects, has lower body wave drag as well as more favorable wing/body interference drag.

The aforementioned aerodynamic studies indicated that, of the favorable aerodynamic concepts investigated, the parasol wing concept offered the greatest aerodynamic potential for Mach 3.0 design applications. Additional aerodynamic studies were then conducted to provide design guidance for developing an airplane configuration incorporating the parasol wing concept. These parasol wing design guideline studies are summarized in the next section.

8.0 Parasol Wing Aerodynamic Design Guidance Studies

Theoretical aerodynamic studies were made to investigate the following parasol wing/body design characteristics:

- Parasol lateral curvature (anhedral/dihedral)effects
- Parasol wing planform area cutout
- Multiple shock reflections
- Body/wing relative incidence effects
- Nacelle parasol characteristics (open nose body)

The theoretical studies were supplemented, where possible, with results of several previously conducted Boeing wind tunnel test programs[38, 39, 40] and available experimental results of other sources[31, 32, 36, 37]. In addition, test/theory comparisons were made to validate the theoretical methods of the parasol wing design and analysis studies.

8.1 Parasol Wing Test/Theory Comparisons

Theoretical predictions were made of the NASA parasol wing wind tunnel model [37], shown in Figure 19.

The test/theory comparisons are shown in Figure 20 for

one of the test Mach numbers. The lift, drag, and lift/drag ratio predictions are quite good. Differences between the experimental and theoretical pitching moment data indicate that the predicted aerodynamic center is further aft than indicated by the test data.

A major difference between the theoretical calculations obtained with FLEXSTAB, and the results obtained with ADASSA, is in the distribution of the interference pressures in the wing. ADASSA predicts the body bow shock wave that forms forward of the Mach wave cone from the body nose. The linear theory results of FLEXSTAB restrict the body influence to the area behind the Mach cone.

The Mach cone at Mach 3.0 from the body nose intersects the parasol wing behind the leading edge. However, the predicted shock wave actually falls in front of the wing leading edge. The ADASSA results, which predict slightly more lift and nose-up pitching moment at zero incidence angle than FLEXSTAB, agree slightly better with the test data.

Results of these test/theory comparisons indicate that both the FLEXSTAB and ADASSA linear theory programs can predict the aerodynamic characteristics of a flat parasol wing configuration.

DESIGN GUIDELINE 1:

- The shock wave locations calculated by ADASSA should be used in the design of a parasol wing planform instead of the FLEXSTAB calculated interference areas.

8.2 Parasol Lateral Curvature

Results obtained using slender body theory in Section 7.0 indicate that parasol wing anhedral can be used to amplify the interference lift. A study was made to determine if FLEXSTAB could predict this effect.

The wing planforms evaluated for this study were derived from the NASA parasol wing planform that was used for the test/theory comparisons. The study planforms are shown in Figure 21. The minimum distance between the body and each planform was held constant. Results of the analyses are shown in Figure 22. The FLEXSTAB results show an increase in interference lift, similar to the slender body theory trends. The parabolic parasol has approximately 50% more interference lift than the flat parasol. The wing struts included in the analysis had a detrimental effect on interference lift.

The lift curve slope, C_{L_α}, decreases for anhedral angles above 30 deg. It should be noted that the wing span for the flat parasol and 30-deg anhedral parasol are nearly equal. The span for the parabolic parasol and 45-deg anhedral parasol are nearly equal to each other, and are less than the spans of the other planforms. These results tend to indicate that the effect of wing anhedral on lift curve slope can be reduced by keeping the wing span constant.

DESIGN GUIDELINE 2:

- Interference lift can be increased by wing anhedral. FLEXSTAB can be used to predict wing anhedral effects on interference lift.

DESIGN GUIDELINE 3:

- A large projected wing span should be maintained to reduce the adverse effects of wing planform lateral curvature (anhedral, dihedral) on lift curve slope.

Wing anhedral increases the surface area of the wing as the projected wing span is held constant. This increases both the friction drag and the thickness wave drag. Hence, the determination of an optimum aerodynamic wing anhedral distribution requires an examination of the net effects on friction drag, wave drag, interference lift, and lift curve slope.

8.3 Parasol Planform Cutout Area

Theoretical surface pressure distributions, bow shock locations, and body interference pressures acting on a planar surface above the body were calculated using ADASSA[6].

The theoretical pressure distributions calculated on a planar wing above a pointed nose body representing a fuselage, and above an open nose body representing an engine nacelle, are shown in Figure 23.

These pressure distributions reveal a negative pressure region, which diminishes the lift produced by the positive pressures. If this region is eliminated, appreciably higher interference lifts can be obtained than the maximum values predicted by slender body theory.

Theoretical predictions of interference lift for planforms tailored to capture only the positive pressures are shown in Figure 24. Interference lift is seen to increase dramatically over the slender body theory maximum value. The results do not indicate a significant effect of the wing/body separation distance. This is because the theory does not account for multiple shock reflections that can increase the interference lift. This is discussed further in the section below.

Note that the wing capture area grows rapidly as the streamwise length increases, or as the parasol height increases. The net effect is that the interference lift coefficient, based on the total wing capture area, decreases with increasing parasol height or streamwise length.

The above results suggest the following design guideline:

DESIGN GUIDELINE 4:

- To minimize the capture area and maximize the interference lift, the wing planform should be designed so that the leading edge matches the body bow shock in the plane of the wing, and the trailing edge cuts off any negative interference pressures on the wing.

8.4 Multiple Shock Reflections

Experimental interference lift data[38, 39, 40] obtained with a number of different body geometries indicate large increases in interference lift as the separation distances are decreased (Figure 25). This is the result of multiple shock reflections between the body and the wing. These shock reflections increased the lift on the wing, but had an insignificant effect on the drag of the bodies.

DESIGN GUIDELINE 5:

- The interference lift can be increased by reducing the gap to permit multiple reflections between the body and wing.

8.5 Wing/Body Incidence Effects

Experimental studies reported in References 32 and 38 investigated the effect of the incidence angle between the wing and body. Results, such as shown in Figure 26, indicate a significant effect on the interference lift. Rotating the body nose-down increases the interference lift. Conversely, increasing the body attitude decreases the interference lift.

DESIGN GUIDELINE 6:

- The interference lift can be increased by mounting the body nose-down relative to the wing. The effect on drag is small.

8.6 Nacelle Parasol vs Body Parasol Studies

Theoretical investigations were made to compare the aerodynamic characteristics of a parasol, designed to capture interference lift from a typical Mach 3.0 nacelle (open nose body), with a parasol designed to capture interference lift from a fuselage (closed nose body).

The calculated wave drag for the nacelle in the presence of a parasol is shown in Figure 27. These results indicate that the nacelle centerline should be located approximately 0.7 to 0.8 of the maximum body diameter below the wing, to achieve maximum wave drag cancellation effects. It also appears that the wave drag of the nacelles can be reduced by 10% to 40%, depending on the parasol lateral curvature.

Results of a similar study for the fuselage were shown in Figure 17. The fuselage must be located approximately 1.5 body diameters below the wing to achieve optimum wave cancellation. This distance is much greater than that required for the nacelle parasol.

The effects of body fineness ratio and inlet area in reducing the parasol/body separation distance necessary to achieve maximum wave drag cancellation are shown in Figure 28.

The experimental data shown previously in Figure 25 indicated that the net interference lift on a wing/nacelle parasol arrangement can be increased above the slender body theory level, if the separation distance in small enough to result in multiple shock reflections. The optimum nacelle/wing separation distance is close enough to allow multiple reflections. Conversely, the optimum separation distance for the body parasol wing arrangement greatly exceeds that for multiple reflections. Hence, the fuselage parasol cannot derive additional interference lift due to multiple reflections without incurring an increase in body wave drag.

DESIGN GUIDELINE 7:

- Lower body fineness ratios reduce the optimum body/wing separation distance.

DESIGN GUIDELINE 8:

- The optimum separation distance for a nacelle parasol is small enough to achieve multiple shock reflections, and, thereby, increase interference lift (design guideline 5). This also results in shorter struts to support the nacelle.

DESIGN GUIDELINE 9:

- The optimum separation distance for a typical fuselage is so large that desirable multiple shock wave reflection between the body/wing will not occur.

DESIGN GUIDELINE 10:

- The forecowl angle of a nacelle offers the capability to increase interference lift. The forecowl angle should be selected to optimize the trade between increased interference lift, and the adverse effects of increased nacelle wave drag and nacelle weight.

8.7 Final Parasol Concept Selection

Wing parasol geometries have been calculated for a typical Mach 3.0 nacelle, and for a fuselage using the aforementioned design guidelines. The results are shown in Figure 29. The body parasol is quite far from the body and would, therefore, require a pair of rather large struts. The nacelles can be supported by a single short strut, thus saving both weight and drag. The wing span for the body parasol is much larger than the span for the nacelle parasol. However, a configuration design incorporating a nacelle parasol on each side of the fuselage would have approximately the same span as the fuselage parasol.

The double-parasol wing configuration, shown conceptually in Figure 29, was selected for the final favorable interference concept. The wing planform geometry for this double-parasol wing concept is derived in the next section.

9.0 Parasol Wing Configuration Evaluation

The double-parasol wing planform was derived using the aforementioned design guidelines. The nacelles are located 0.8 body diameters below the wing chord plane.

The wing planform was designed to capture the nacelle interference pressures. The projected hyperbolic wing planform shape is designed for the maximum amount of nacelle interference lift per unit wing area.

The planform curvature in the front view was designed to enhance the interference lift generation. The planform has a parabolic curvature between the nacelle and the body, and an additional parabolic section near the wing tip. The nacelle is at the focus of each parabolic section. The flat midwing section provides additional wing span and greater lift capture area.

The nacelles are tilted down, relative to the wing, to better align the inlets with the free stream, and to increase the interference lift. The wing leading edge inboard of the nacelle increases the wing root chord, and blends into the leading edge determined from the bow shock location calculations. The final parasol wing planform is shown in Figure 30, with the Mach 3.0 design interference lift areas.

The wing camber and twist have been designed to minimize the unfavorable nacelle/wing interference drag. The body has been area ruled to optimize the body/nacelle and body/wing interference effects.

The double-parasol wing favorable interference configuration, shown in Figure 30, is representative of a Mach 3.0 small supersonic military aircraft.

9.1 Aerodynamic Evaluation

The double-parasol wing configuration was analyzed using ADASSA, FLEXSTAB, and empirical data for leading-edge suction corrections at low off-design Mach numbers. ADASSA was used for the volume wave drag, drag due to lift, trim, and friction drag. FLEXSTAB was used to calculate planform lateral curvature effects on interference lift, and on lift curve slope. The computer representation of the configuration used for the aerodynamic analyses is shown in Figure 31.

Calculated lift curve slopes and maximum lift/drag ratios for the double-parasol wing configuration are compared in Figure 30 with corresponding values for a conventional type aircraft designed[5] for the same mission requirements. The reference conventional aircraft had a flat wing design. The effect of incorporating an optimized conventional wing camber and twist is also shown.

The lift curve slope of the double-parasol wing configuration exceeds that of the conventional reference airplane, because of its higher aspect ratio and lower wing sweep.

The double-parasol wing configuration at the Mach 3.0 design condition offers a potential improvement in the lift/drag ratio of approximately 25% relative to the reference flat wing configuration. Optimizing the nacelle area growth of the parasol wing configuration increases the potential lift/drag improvement to 37%. This increase is approximately 20% greater than the lift/drag ratio of the conventional aircraft with an optimized wing design. Additional theoretical and coordinated experimental studies will be necessary to fully identify the potential aerodynamic benefits of the configuration concept.

9.2 Nacelle Design Modification

The double conical shape of the nacelle for the parasol wing configuration results in large negative pressures associated with the nacelle boattail. At the Mach 3.0 design condition, this negative pressure field falls aft of the wing trailing edge. The shock wave pattern from the nacelle moves forward on the wing at lower supersonic Mach numbers. Hence, areas of negative pressures fall on the wing and tend to reduce the interference lift.

The body design procedure of Reference 41 was used to design a modified axisymmetric nacelle, to eliminate the negative nacelle boattail pressures. The modified nacelle requires a substantial increase in the nacelle exit area to eliminate the boattail pressures. A possible alternative aerodynamic solution is the nonsymmetric nacelle design that matches the area growth of the top half of the modified nacelle, but has an exit area equal to the original nacelle. Both modified nacelle designs, however, would affect the propulsive efficiency of the nacelle. Appropriate design trade studies are required to develop a design to balance the trade between engine efficiency and off-design aerodynamic performance.

10.0 Conclusions

The purpose of the study was to identify various ways that favorable interference can increase the aerodynamic efficiency of supersonic aircraft. Comparisons were made between the aerodynamic and weight characteristics of a reference conventional type configuration, and a favorable interference concept incorporating a double-parasol wing concept.

Major conclusions of the study that apply specifically to a small supersonic aircraft include:

- The parasol wing concept was identified as offering the greatest potential aerodynamic benefits, relative to the other concepts considered (wave riders, supersonic biplanes, flat-top wing/bodies).

- The best aerodynamic concept is very dependent upon the design Mach number. The interference concepts considered in this study become more difficult to integrate into a viable aircraft configuration as the design Mach number is reduced.

- More aerodynamic design and detailed design studies are necessary to assess the potential of the double-parasol wing airplane concept.

- Existing aerodynamic and design tools, ADASSA and FLEXSTAB, can predict the force and moment characteristics of flat parasol wing configurations.

- FLEXSTAB can predict lateral curvature effects on interference lift in agreement with slender body theory predictions. However, ADASSA, which uses

Whitham's theory to predict body shocks, is more accurate than FLEXSTAB for predicting the interference pressure patterns that are necessary for the design of the parasol wing planform.

- Study results presented in this paper have considered only the aerodynamic potential of various aerodynamic concepts. A total airplane assessment must consider all aspects of a configuration design, such as weights, structures, engine efficiencies, costs, and flight dynamics for all flight conditions.

Acknowledgements

Results that have been presented in this paper are based on the aerodynamic work supporting the Supersonic Favorable Interference Applications study. This work was performed by The Boeing Company, under the technical direction of P. R. Gord, Air Force Flight Dynamics Laboratory/FXG, Wright-Patterson Air Force Base, Ohio. Dr. H. Yoshihara of The Boeing Company was the program manager.

The author also gratefully acknowledges the contributions of B. J. Lord in assisting with aerodynamic studies, and G. O. Friebel in designing the double-parasol wing configuration.

References

1. *Proceedings of the SCAR Conference NASA CP-001,* Vol I and Vol II, NASA-Langley Research Center, November 1976.

2. *Design Conference Proceedings: Technology for Supersonic Cruise Military Aircraft,* Vol I and Vol II, USAF Academy, Colorado Springs, Colorado, February 1976.

3. Kane, E.J., and Middleton, W.D., (1970): *Considerations of Aerodynamic Interference in Supersonic Airplane Design,* Paper No. 3, AGARD Conference Proceedings No. 71, September 1970.

4. Sigalla, A., and Hallstaff, T. H. (1967): "Aerodynamics of Powerplant Installations on Supersonic Aircarft," *Journal of Aircraft,* pp 273–277, July–August 1967.

5. Kulfan, R.M., Friebel, G.O., Lord B.J., and Yoshihara, H., (1978): *Application of Supersonic Favorable Aerodynamic Interference to Fighter Type Aircraft.* AFFDL-TR-78-33, April 1978.

6. Middleton, W.D., and Lundry, J.L., (1976): *A Computational System for Aerodynamic Design and Analysis of Supersonic Aircraft,* NASA Contract NAS1-13732, NASA CR-2715, (Boeing Program A389), July 1976.

7. Dusto, A. R., et al., (1974): *A Method for Predicting the Stability Characteristics of an Elastic Airplane, Vol I FLEXSTAB Theoretical Manual,* NASA CXR 114712, 1974.

8. Kuchemann, D., (1962): "Aircraft Shapes and Their Aerodynamics for Flight at Supersonic Speeds," In: *Advances in Aeronautical Sciences,* Zurich, 1960, Vol II, pp 221–252, Pergomon Press, Oxford, 1962.

9. Kuchemann, D., (1965): "Hypersonic Aircraft and Their Aerodynamic Problems," In: *Progress in Aeronautical Sciences,* Vol 6, 1965.

10. Ridder, S., (1971): *On the Induced Drag of Thin Plane Delta Wings–An Experimental Study of the Spanwise Distribution of the Leading-Edge Forces at Low Speeds,* Royal Institute of Technology, Technical Note KTH AERO TN57, 1971.

11. Kulfan, R. M., and Sigalla, A, (1978): *Real Flow Limitations in Supersonic Airplane Design,* AIAA Paper 78-147, January 1978.

12. Beane, B.J., *Notes on the Variation of Drag with Mach Number of a Busemann Biplane,* Douglas Aircraft Rep., S.M. 18737.

13. Graham, E. W., et al., (1957): *A Theoretical Investigation of the Drag of Generalized Aircraft Configurations in Supersonic Flow,* NASA TM 1421, January 1957.

14. Graham, M. E., (1955): *Application of Drag-Reduction Methods to Supersonic Biplanes,* Douglas Aircraft Company Report No. SM-19258, September 1955.

15. Licher, R.M., (1955): *Optimum Two-Dimensional Multiplanes in Supersonic Flow,* Douglas Aircraft Rep. S.M. 18688, 1955.

16. Flower, J. W., (1963): "Configurations for Higher Supersonic Speeds Derived from Simple Shock-Waves and Expansions," *Journal of R.A.S.,* May 1963.

17. Nonweiler, T., (1963): "Delta Wings of Shapes Amenable to Exact Shock Wave Theory," *Journal of R.A.S.,* Vol 67, pp 39–40, January 1963.

18. Peckham, D. H., (1962): *On Three-Dimensional Bodies of Delta Planform Which Can Support Plane Attached Shock Waves,* A.R.C. C.P. No. 640, March 1962.

19. Squire, W.C., (1964): *Pressure Distributions and Flow Patterns at M = 4.0 on Some Delta Wings,* ARC R&M No. 3373, 1964.

20. Squire, L.C., (1967): *"Calculated Pressure Distributions and Shock Shapes on Thick Conical Wings at High Supersonic Speeds,"* Aeronautical Quarterly, Vol XVIII, Part 2, pp 185-206, May 1967.

21. Goldsmith, E.L., and Cook, P.H., (1964): *Some Mutual Interference Effects Between a 5.7° Cone and a Sonic L.E. Delta Wing at M = 2.49,* R.A.E. Tech. Note No. Aero 2936, 1964.

22. Eggers, A. J., Jr., and Syvertson, C. A., (1956): *Aircraft Configurations Developing High Lift Drag Ratios at High Supersonic Speeds,* NACA RM A 55L05, 1956.

23. Eggers, A. J., Jr., (1960): "Some Considerations of Aircraft Configurations Suitable for Long-Range Hypersonic Flight," In: *Hypersonic Flow* (Editors A. R. Collar and J. Tinkler) Butterworth, London.

24. Goldsmith, E. L., and Cook, P. H., (1965): *Half Body and Wing Combinations in Supersonic Flow: A Review of Some Principles and Possibilities,* R.A.E., Tech. Report 65040, 1965.

25. Boyd, J. A., (1965): *Optimal Utilization of Supersonic Favorable Interference to Obtain High Lift-Drag Ratios,* AIAA Paper 65-752, November 1965.

26. Brown, C.E., and McLean, F.E., (1959): *"The Problem of Obtaining High Lift-Drag Ratios at Supersonic Speeds,"* J.A.S., pp 298-302, May 1959.

27. Sigalla, A., (1959): *The Optimization for Minimum Wave Drag of a Fuselage Located Under a Wing,* Boeing Airplane Company Report D6-5189, December 1959.

28. Chen, C. F., and Clarke, J. H., (1960): *A Study of Configurations Composed of a Body Under a Lifting Wing in Supersonic Flow,* Division of Engineering, Brown University, Air Force Office of Scientific Research TN 59-1276, 1960.

29. Chen, C. F., and Clarke, J. H., (1961): "Body Under Lifting Wing," *J.A.S.,* Vol 28, No. 7, pp 547–562, July 1961.

30. Clarke, J. H., (1959): *The Forces on Wing-Fuselage Combinations in Supersonic Flow,* Boeing Document D1-82-0018, August 1959.

31. Cook, P. H., (1966): *Further Experimental Results on the Mutual Interference Between Separated Wings and Bodies at M = 2.49,* R.A.E. Tech. Report No. 66228, July 1966.

32. Gapcynski, J. P., and Carlson, H., (1954): *A Pressure-Distribution Investigation of the Aerodynamic Characteristics of a Body of Revolution in the Vicinity of a Reflection Plane at Mach Numbers of 1.41 and 2.01,* NACA RM-L54J29, October 1954.

33. Graham, E. W., and Licher, R. M., (1959): *The Calculation of Interference Drag Between Wing Lift and Fuselage Thickness at Supersonic Speeds,* Douglas Aircraft Report No. SM-23446, February 1959.

34. Jones, R. T., (1957): *Minimum Wave Drag for Arbitrary Arrangements of Wings and Bodies,* NACA TN 1335, 1957.

35. Ferri, A., Clarke, J.H., and Ting, L., (1957): "Favorable Interference in Lifting Systems in Supersonic Flow, *J.A.S.,* Vol. 24, No. 11, pp 791-804, November 1957.

36. Morris, O. A., and Lamb, M. (1968): *Aerodynamic Characteristics in Pitch of a Modified Half-Ring-Wing-Body Combination and a Swept Wing-Body Combination at Mach 2.16 to 3.70,* NASA TM X-1551, April 1968.

37. Morris, O.A., and Mack, R.J., (1968): *Aerodynamic Characteristics of a Parasol-Wing-Body Combination Utilizing Favorable Lift Interference at Mach Numbers from 3.00 to 4.43,* NASA TN D-4855, October 1968.

38. Mysliwetz, F., (1960): *Supersonic Interference of a Body Under a Wing,* Boeing Document D6-5207, July 1960.

39. Mysliwetz, F., Supersonic Interference Lift of a Body-Wing Combination, *AIAA Journal,* Vol. 1 pp 1432–1434, June 1963.

40. Woodward, F. A., (1962): *Pressures and Forces on Wings and Bodies in Close Proximity at Supersonic Speeds,* Boeing Document D6-8927, April 1962.

41. Barger, R.L.: Procedures for Designing Supersonic Bodies of Revolution from Prescribed Pressure Distributions, Paper No. 4, in *Analytic Methods in Aircraft Aerodynamics* NASA SP-228, October 1969.

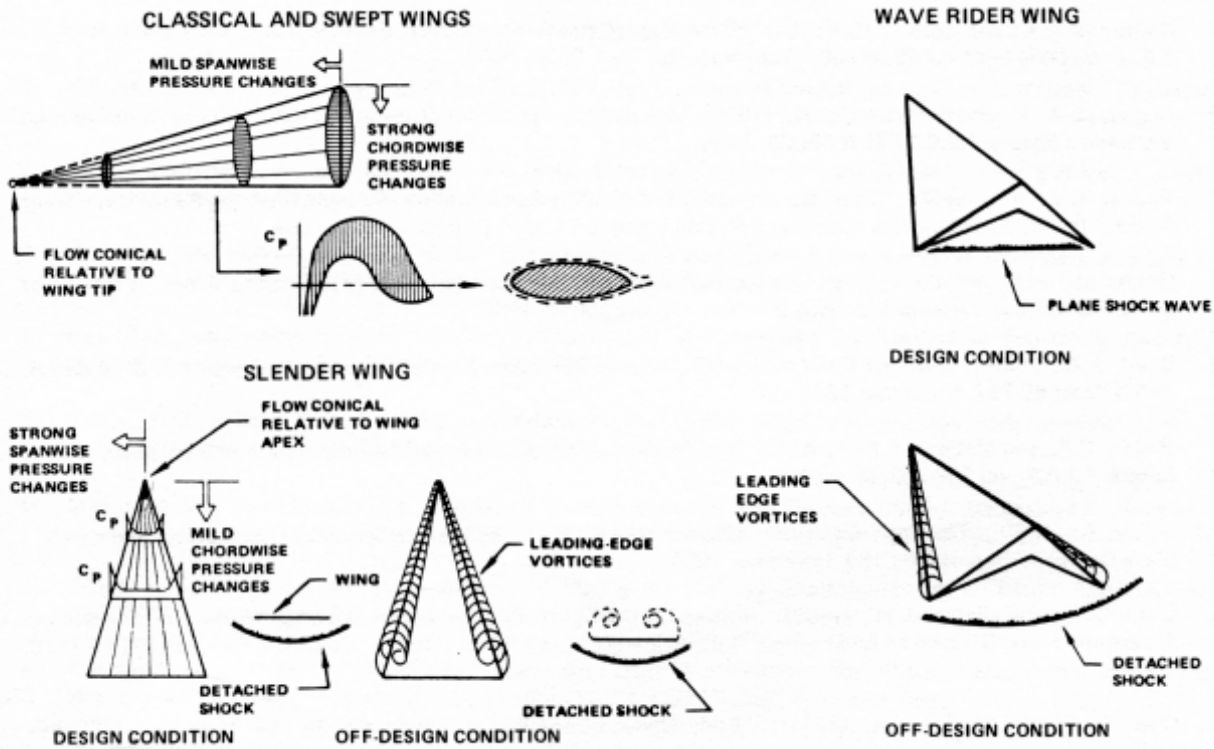

Figure 1. Types of Flow on Wings

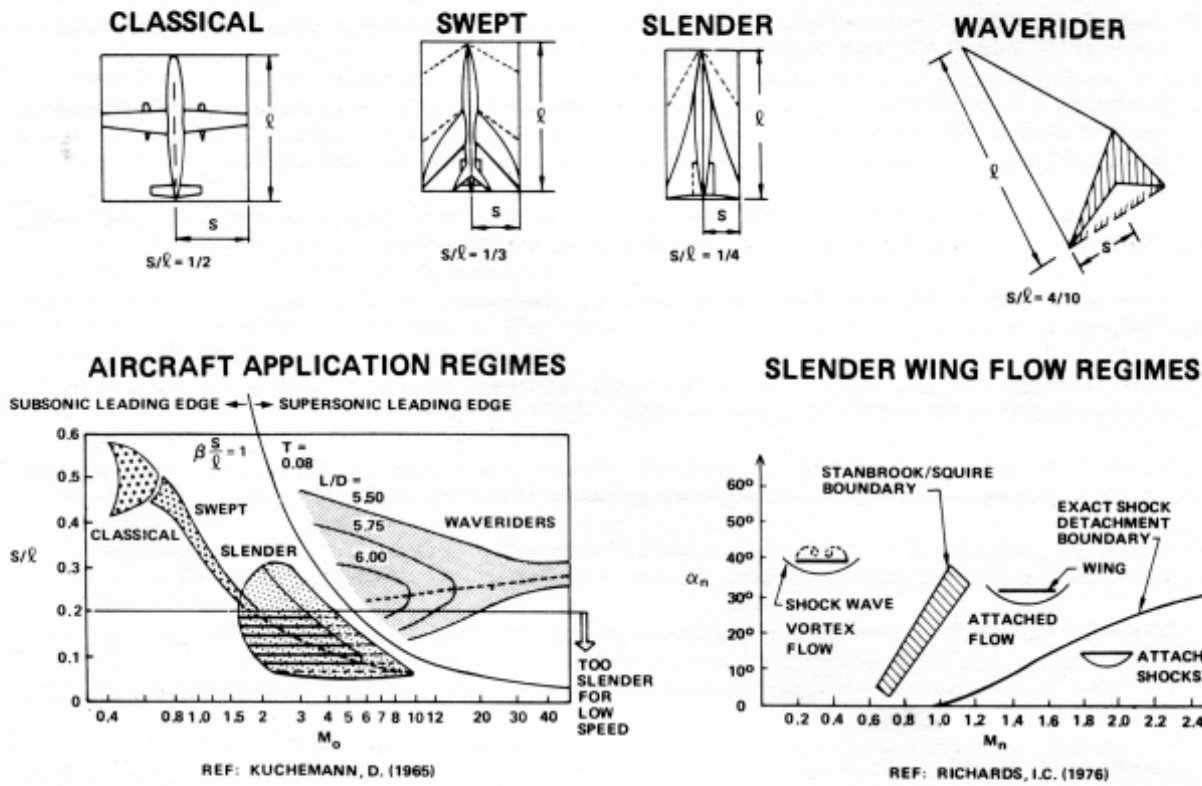

Figure 2. Types of Aircraft

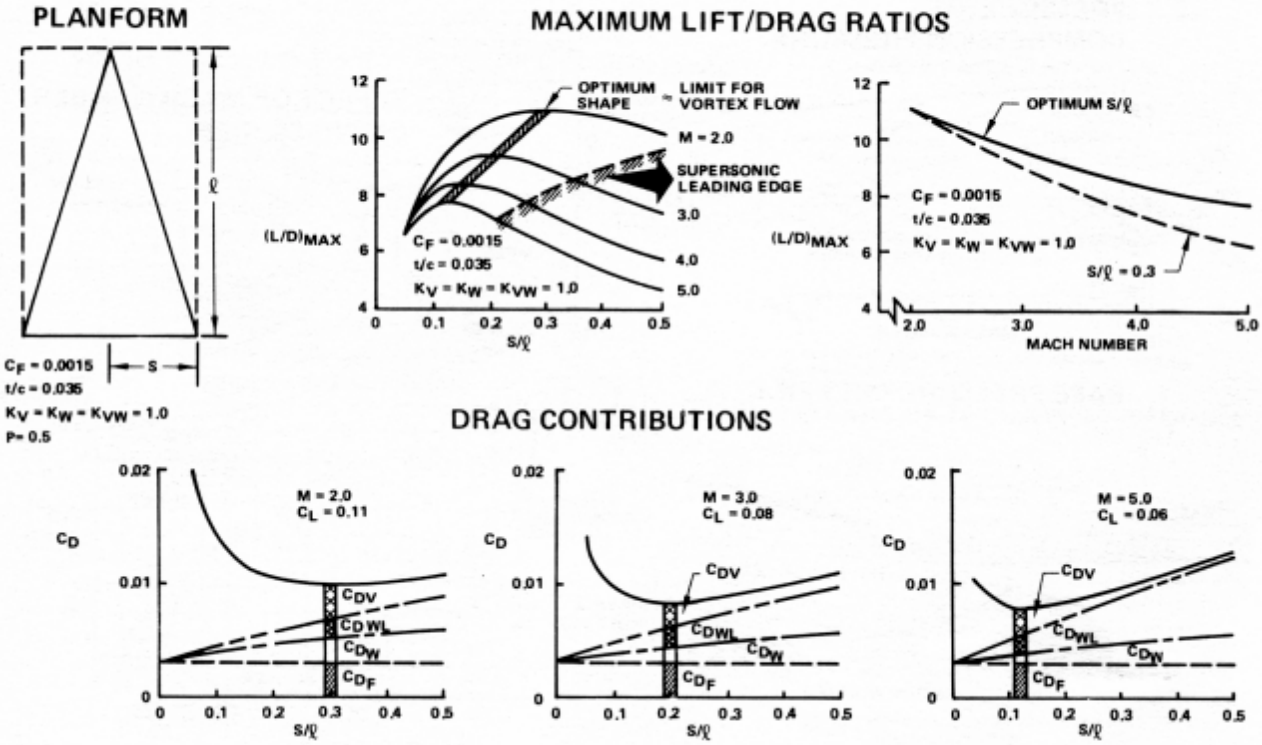

Figure 3. Slender Wing Supersonic Cruise Aerodynamics

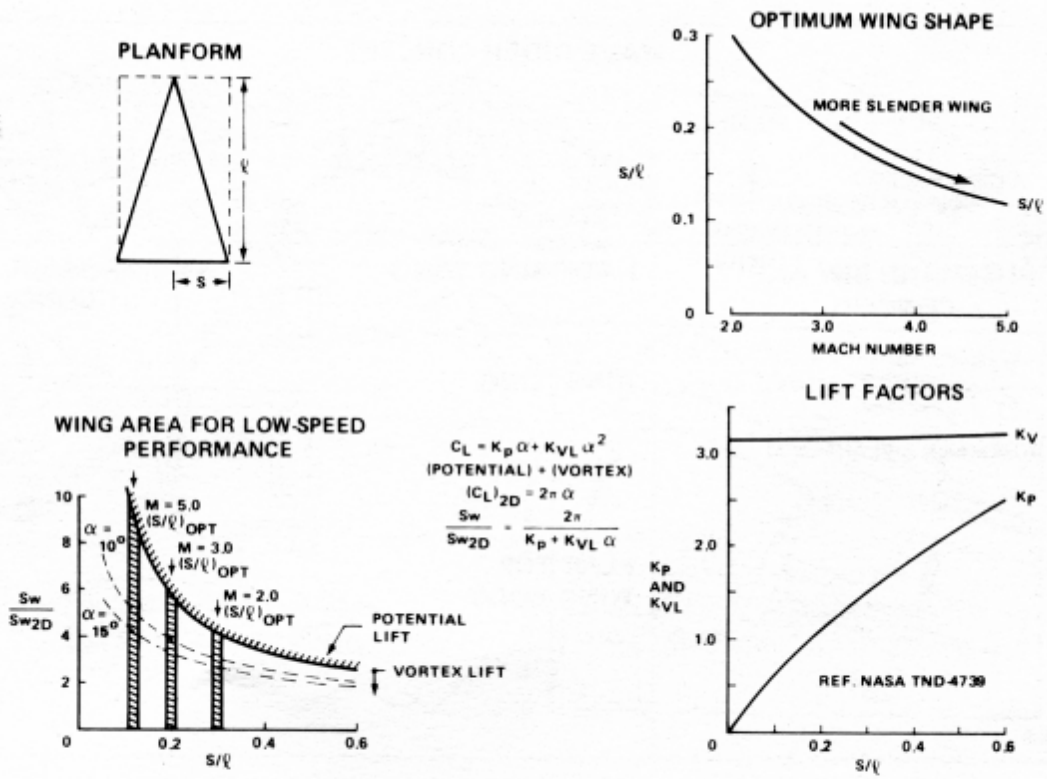

Figure 4. Slender Wing Low-Speed Lift Requirements

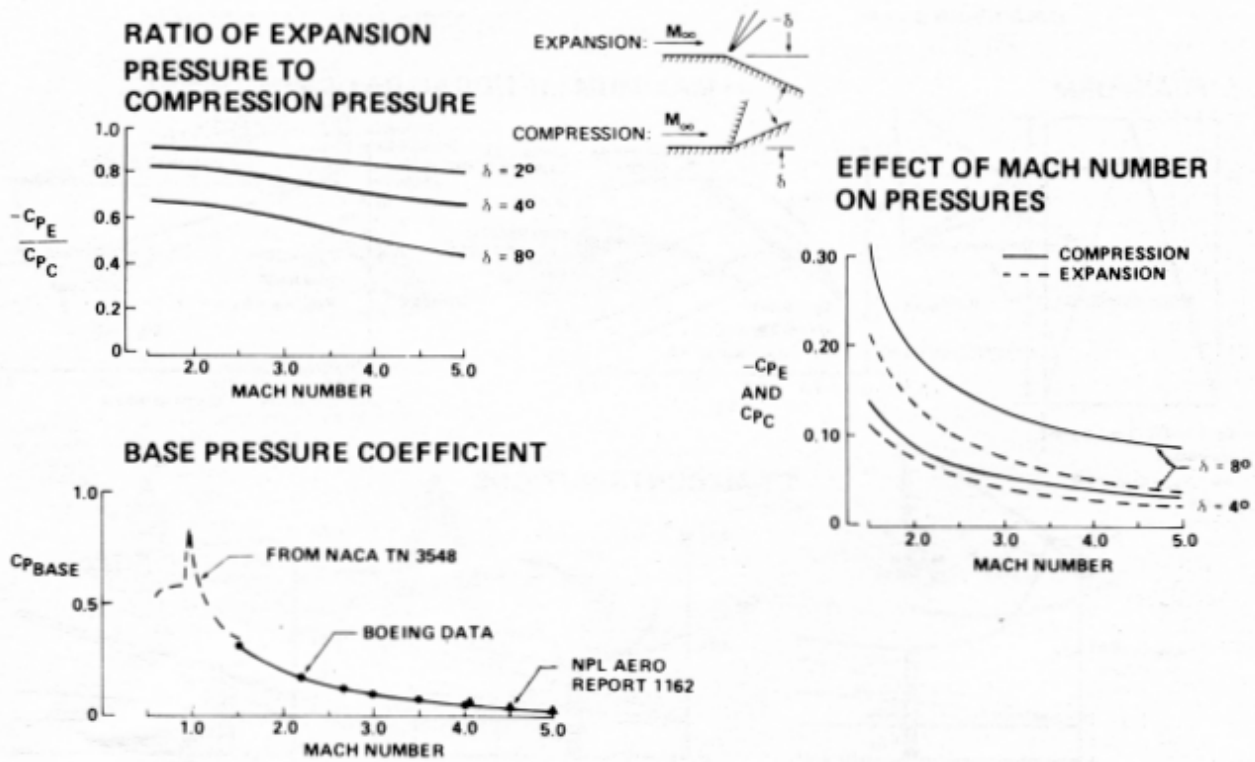

Figure 5. Hypersonic Configuration Aerodynamic Considerations

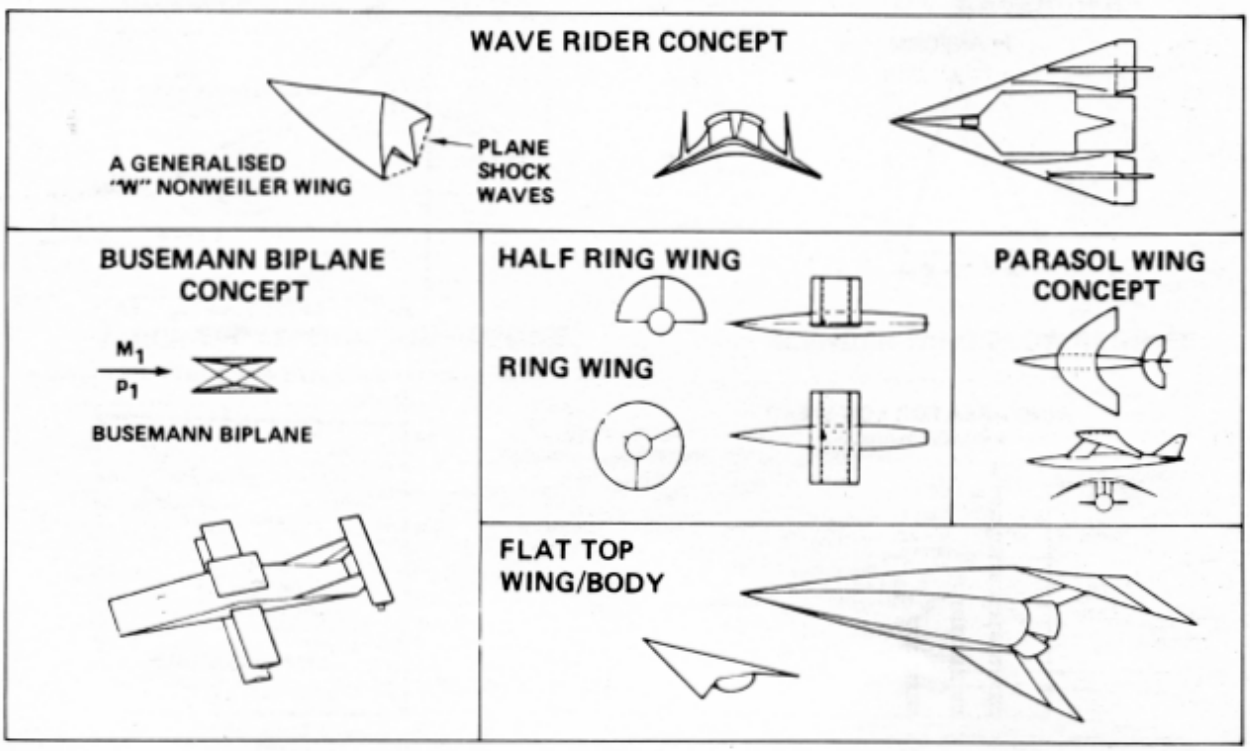

Figure 6. Hypersonic Favorable Interference Concepts

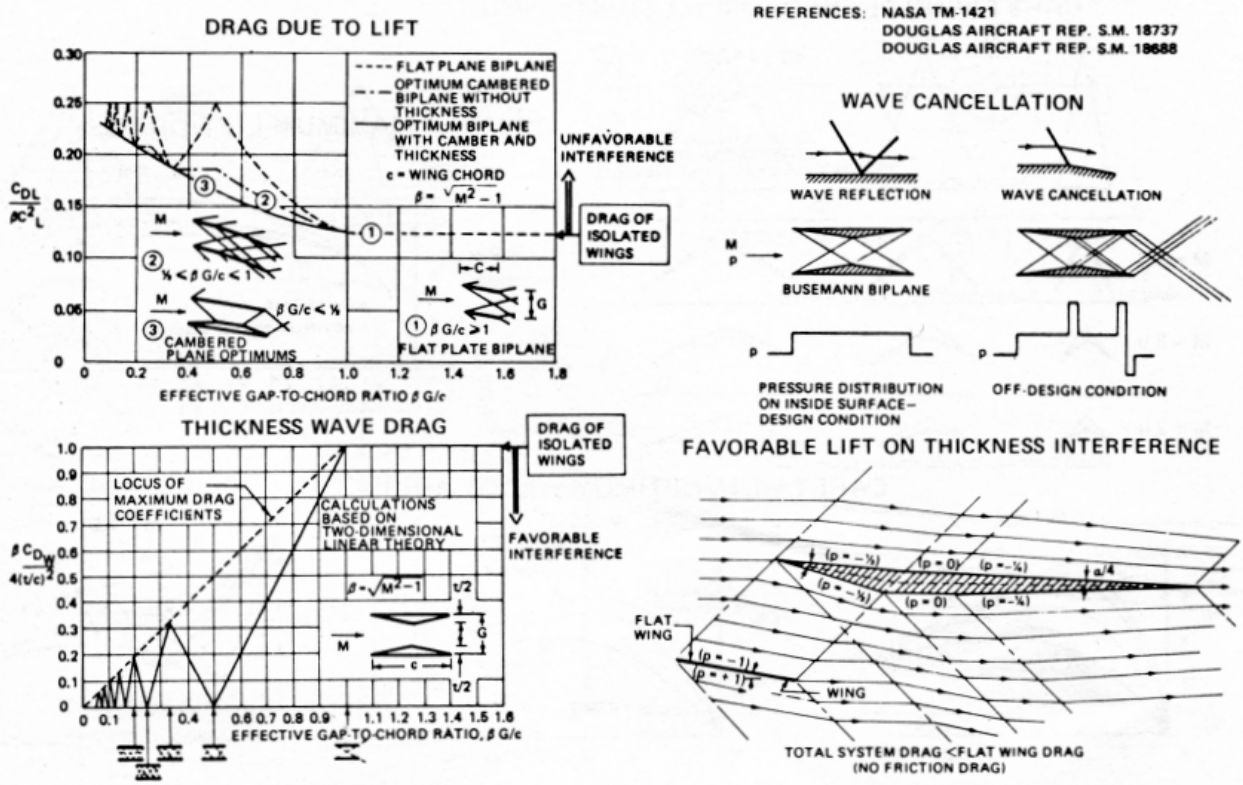

Figure 7. Busemann Biplane Aerodynamics

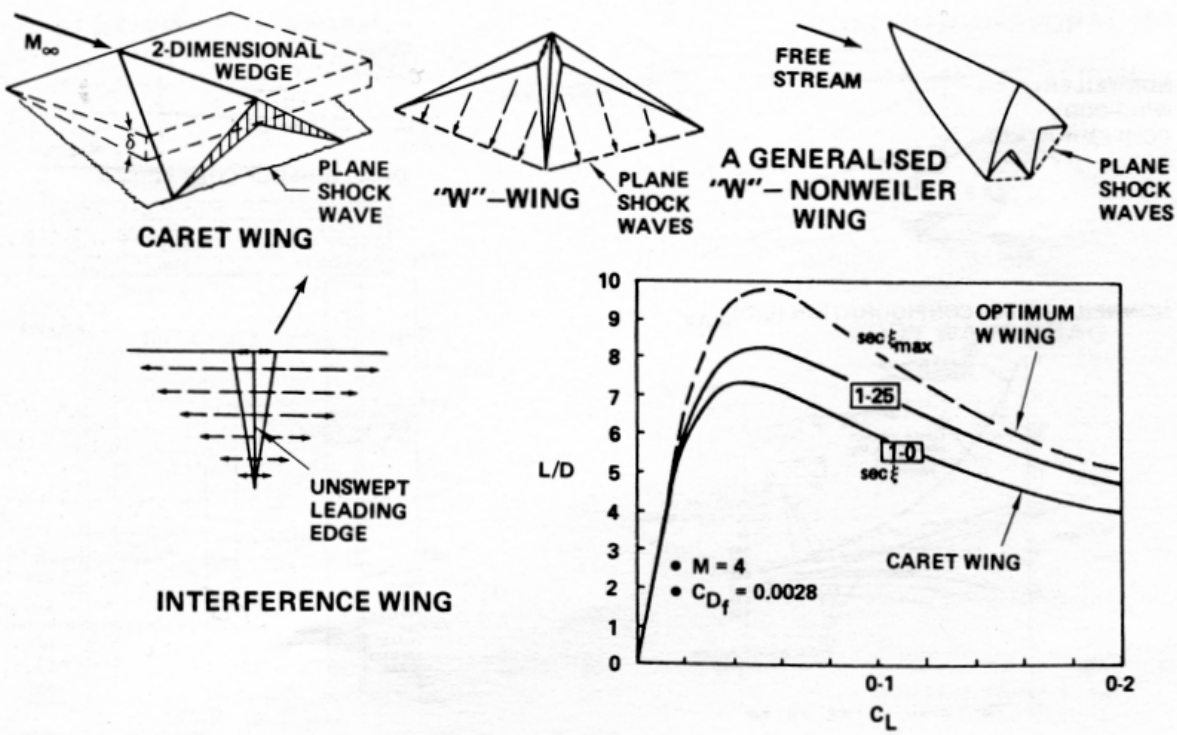

Figure 8. Caret and Nonweiler Wing Aerodynamics

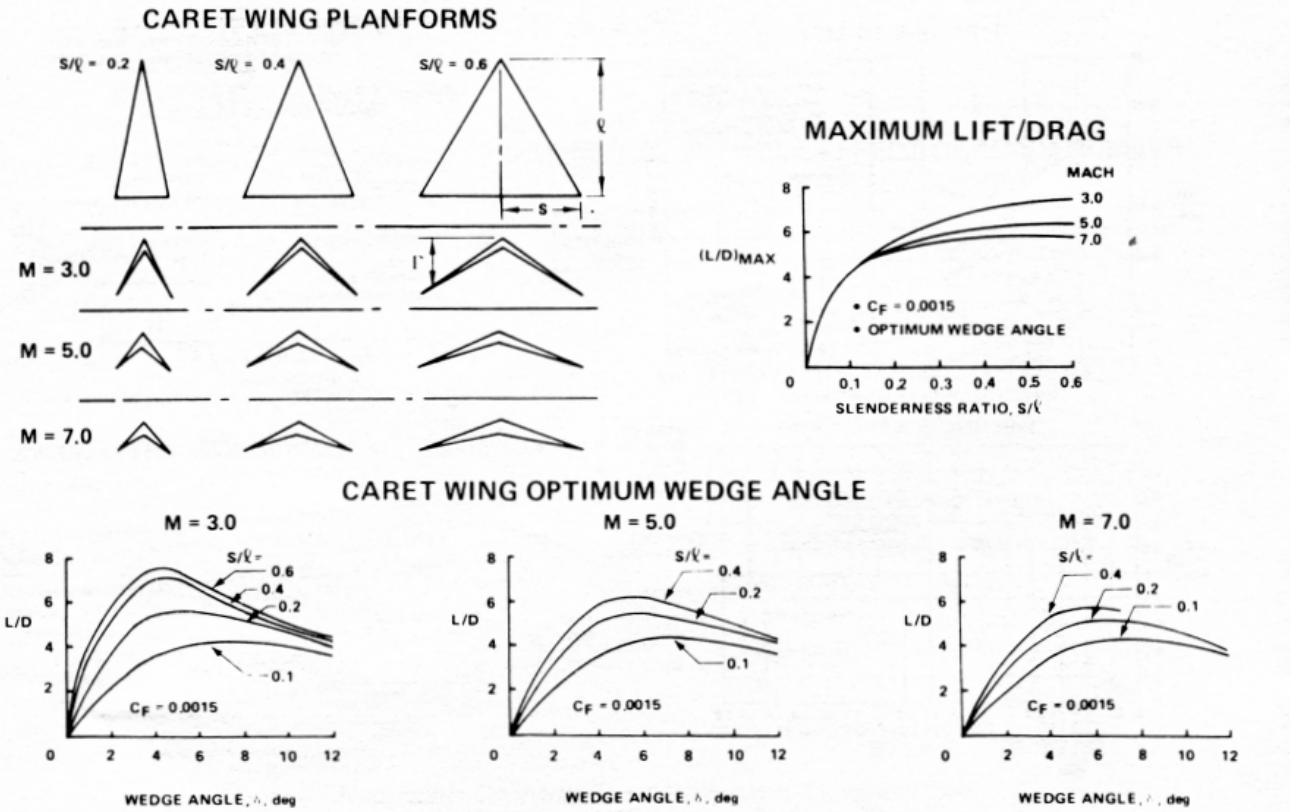

Figure 9. Optimum Caret Wing Characteristics

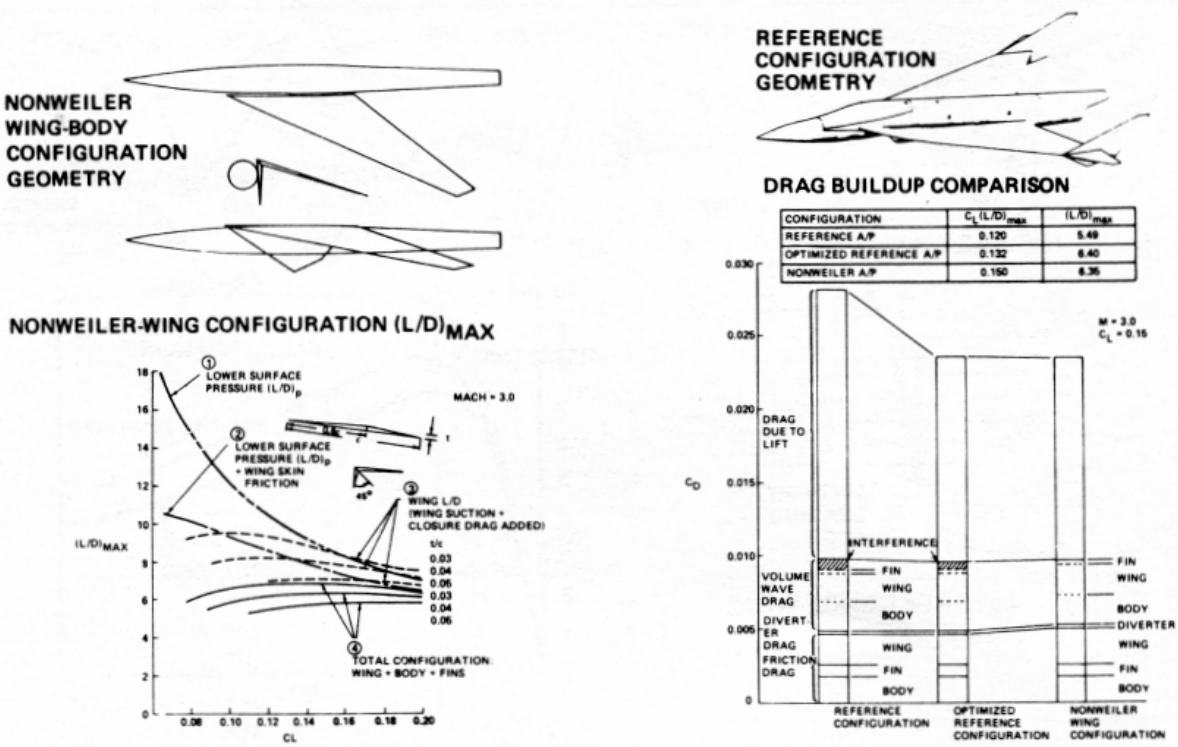

Figure 10. Nonweiler Wing Configuration Evaluation

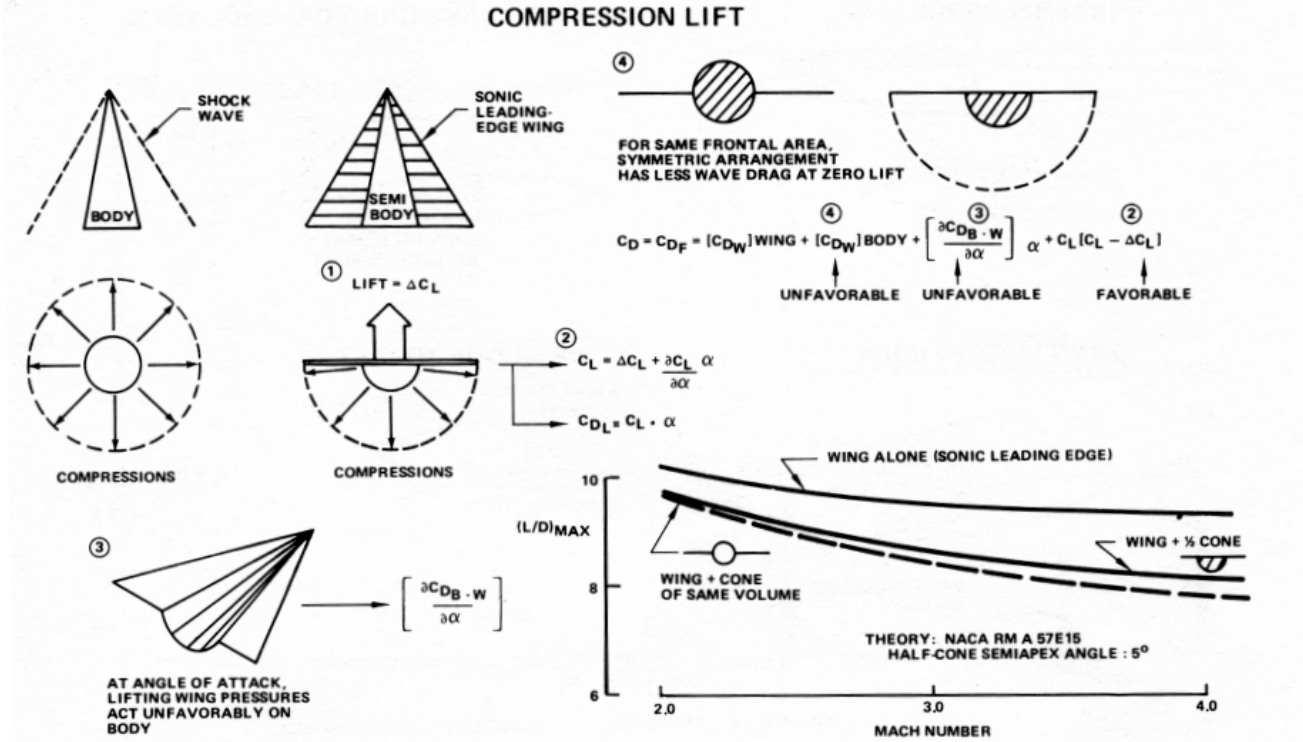

Figure 11. Flat-Top Wing/Body Aerodynamics

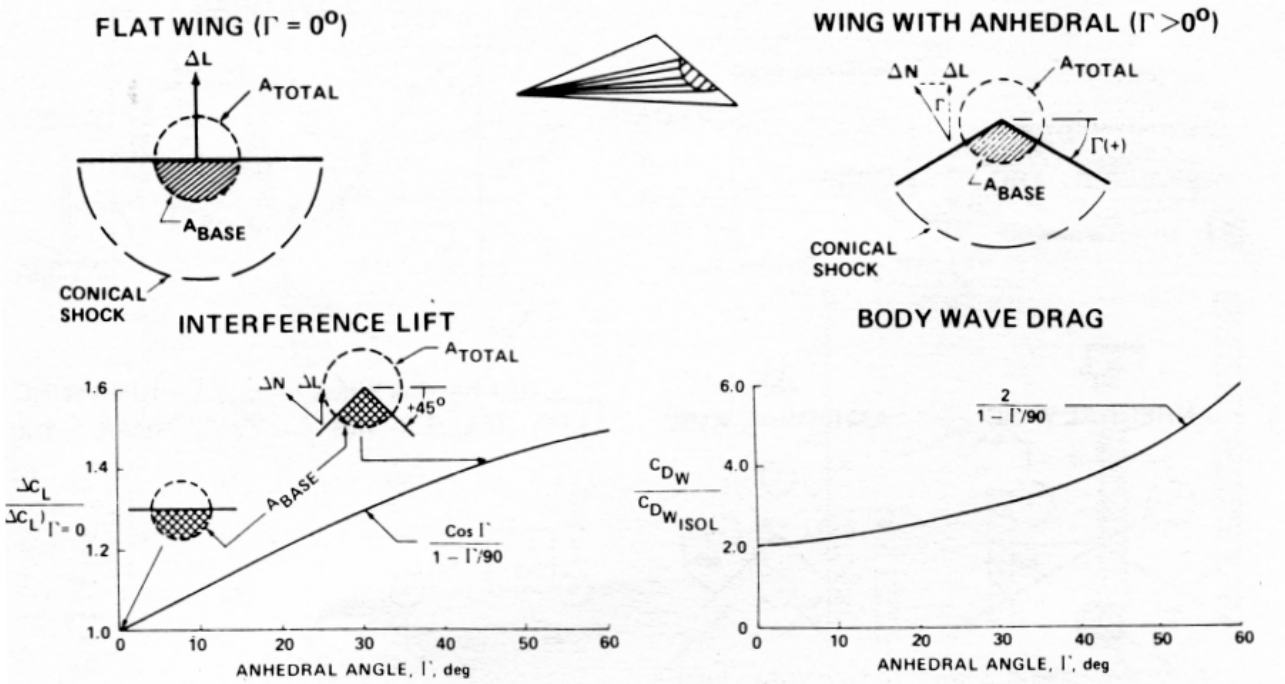

Figure 12. Effect of Anhedral on Flat-Top Wing/Body Lift and Drag

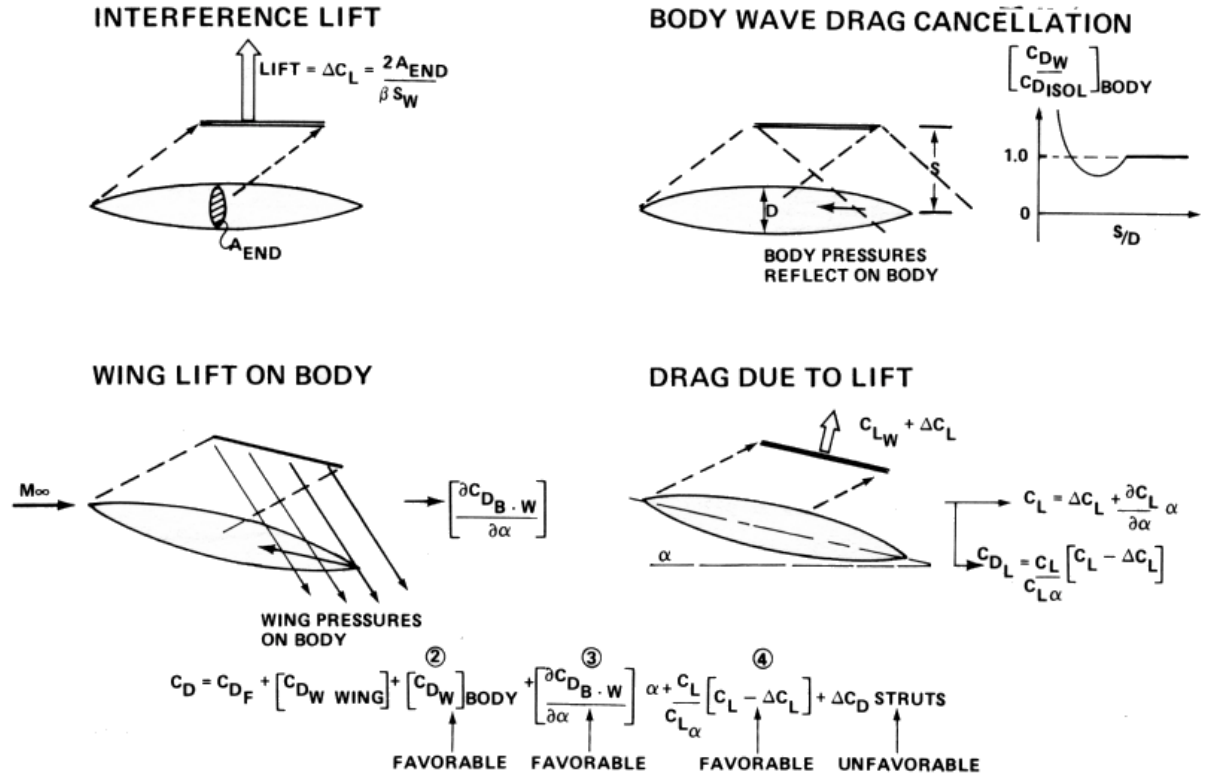

Figure 13. Parasol Wing Aerodynamics

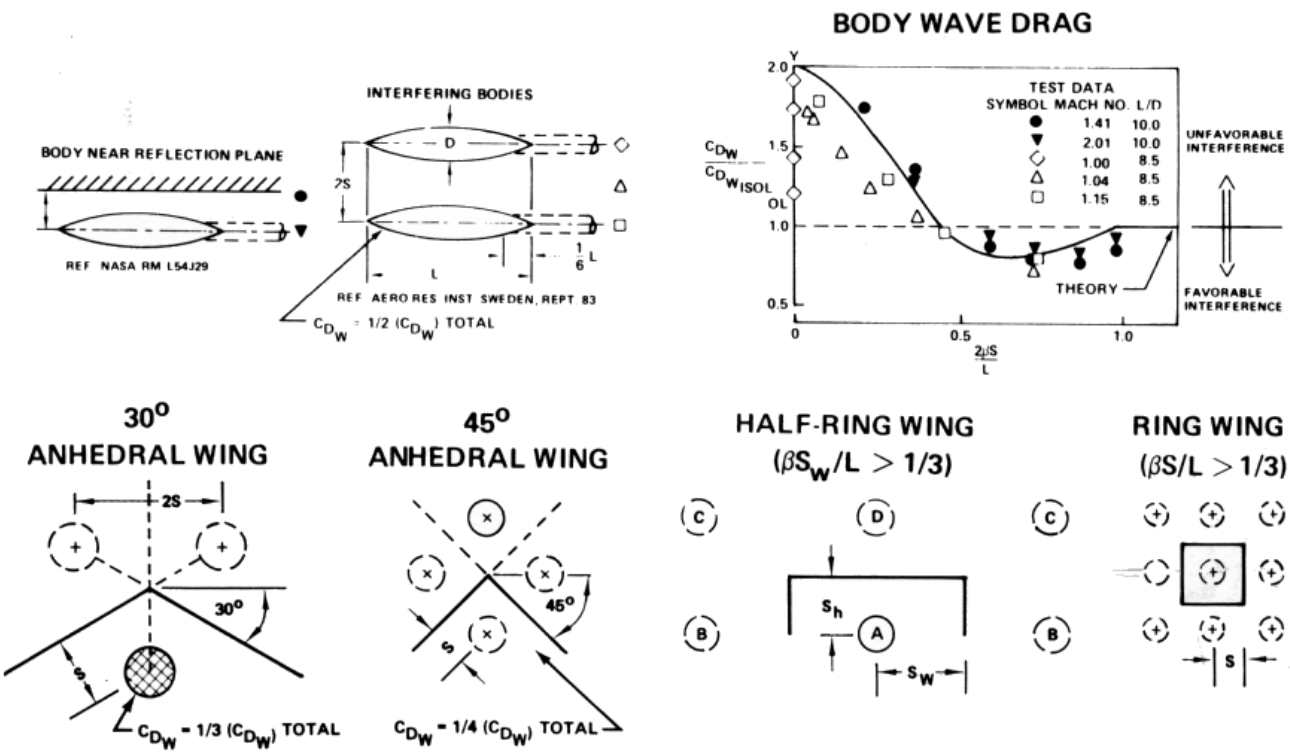

Figure 14. Body Wave Drag Cancellation

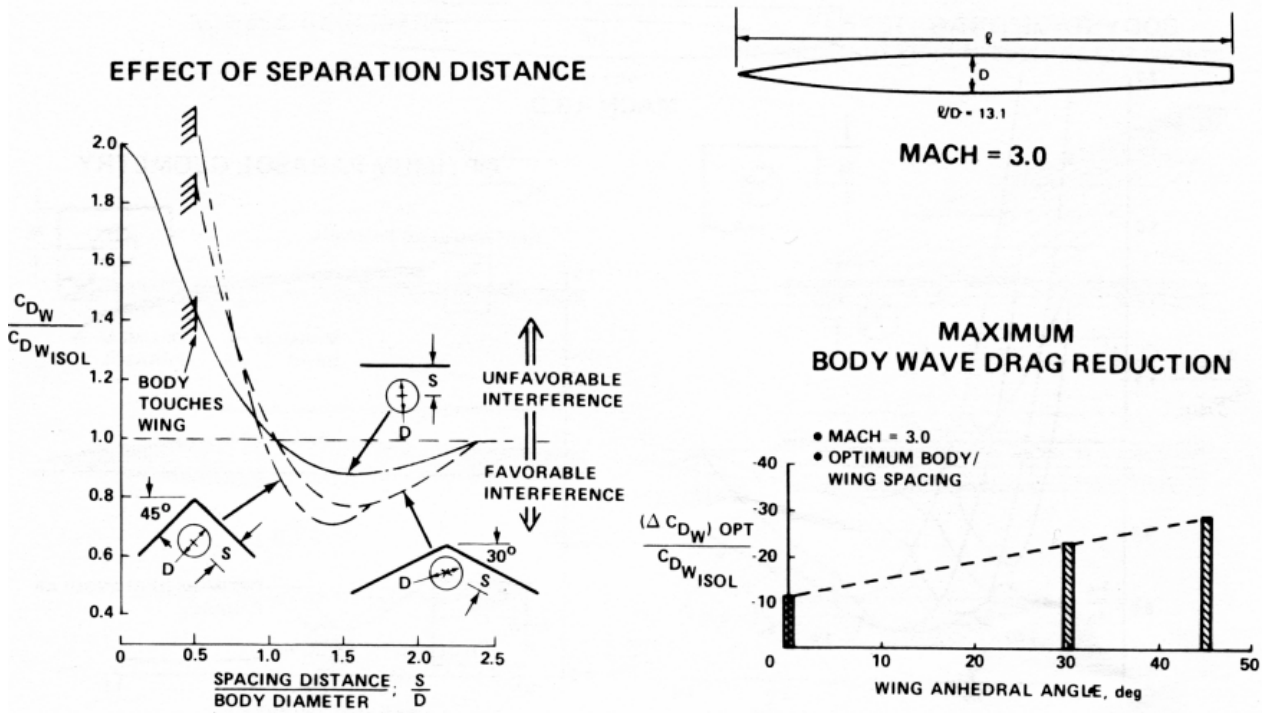

Figure 15. Effect of Anhedral on Body Wave Drag

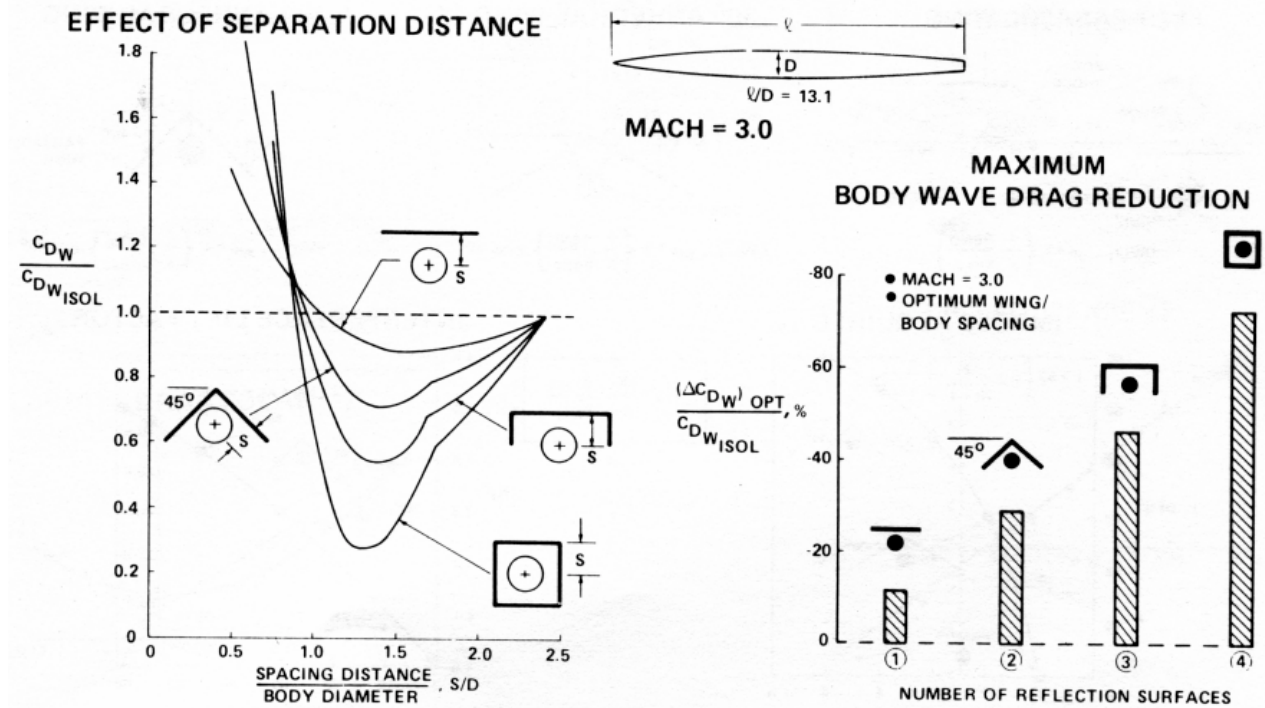

Figure 16. Ring Wing and Parasol Wing/Body Wave Drag Cancellation

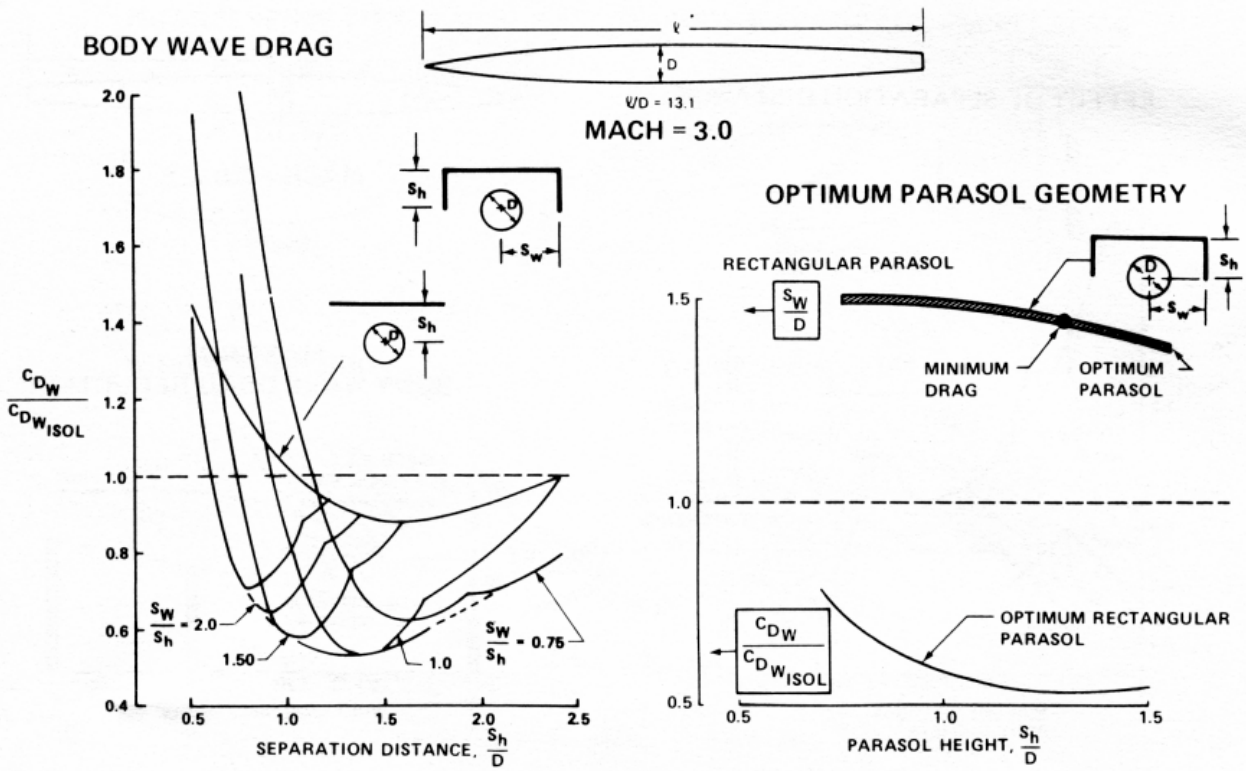

Figure 17. Optimum Rectangular Parasol Geometry

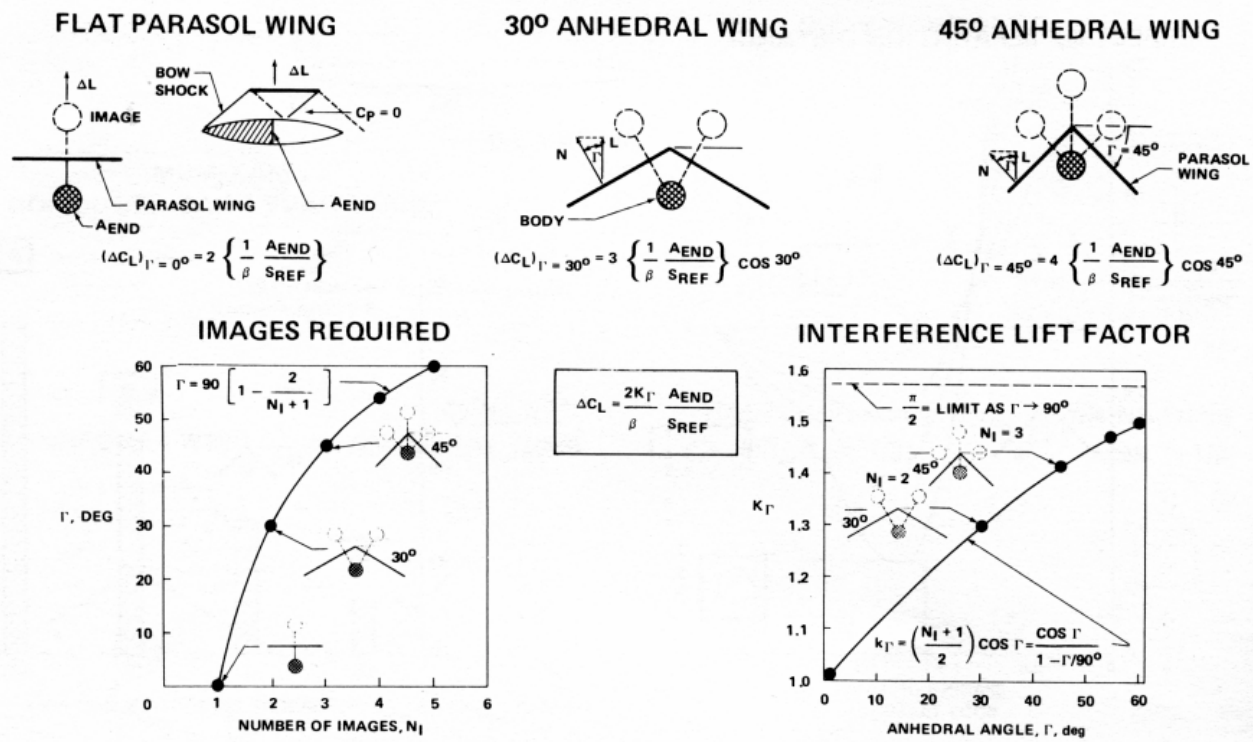

Figure 18. Effect of Anhedral Angle on Parasol Wing Interference Lift

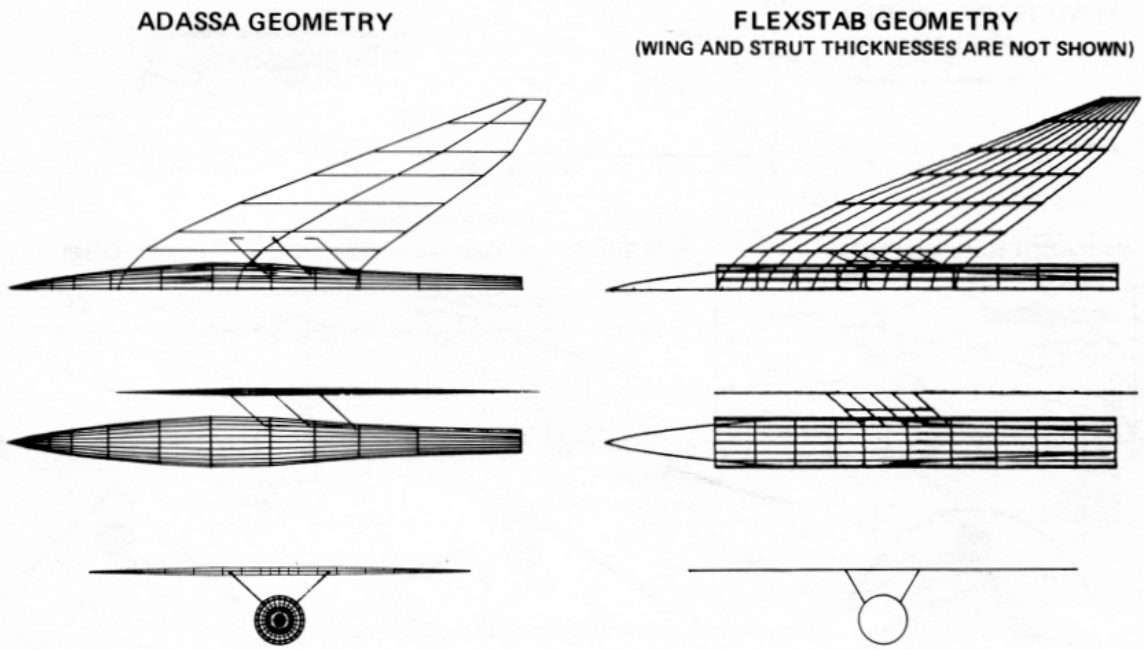

Figure 19. Analytical Representations of the NASA Parasol Wing Wind Tunnel Model

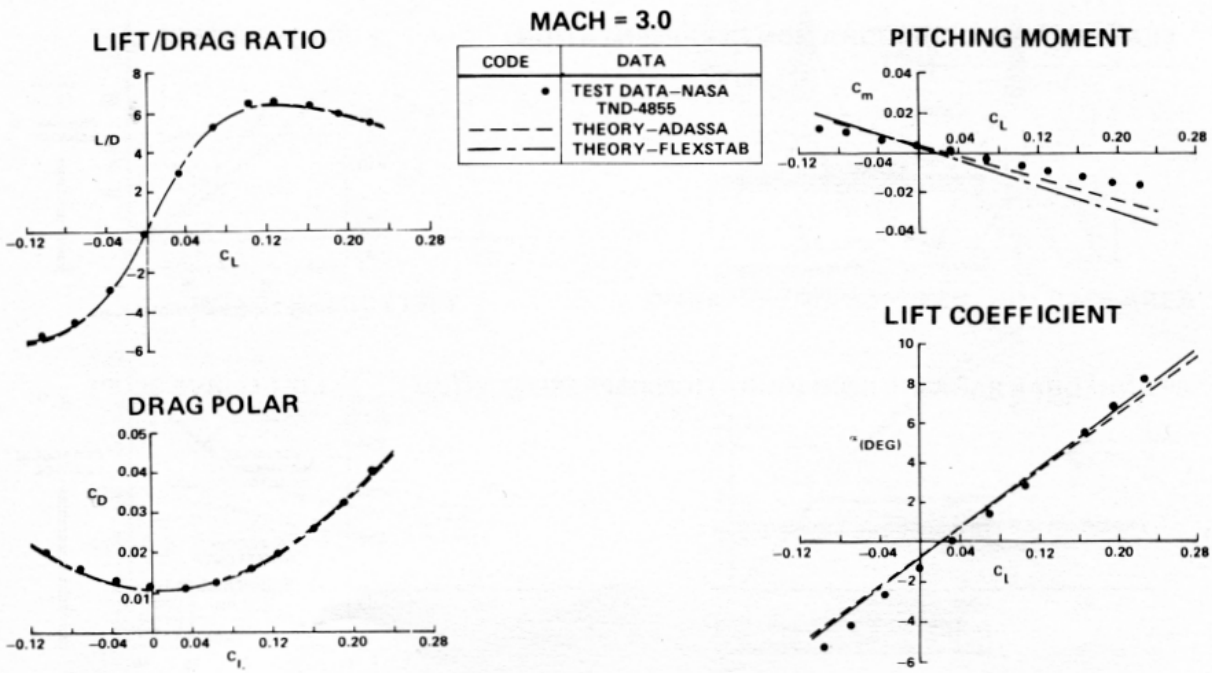

Figure 20. NASA Parasol Wing Wind Tunnel Model Test vs Theory Comparisons

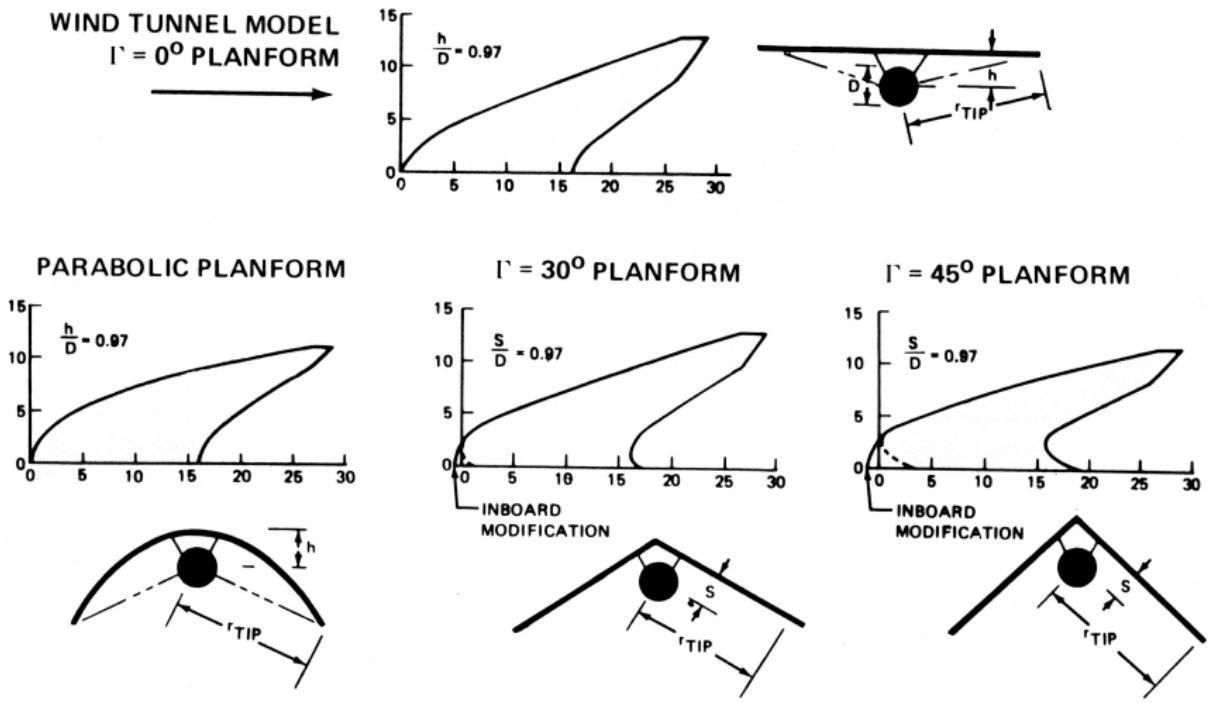

Figure 21. Planforms for Parasol Curvature Study

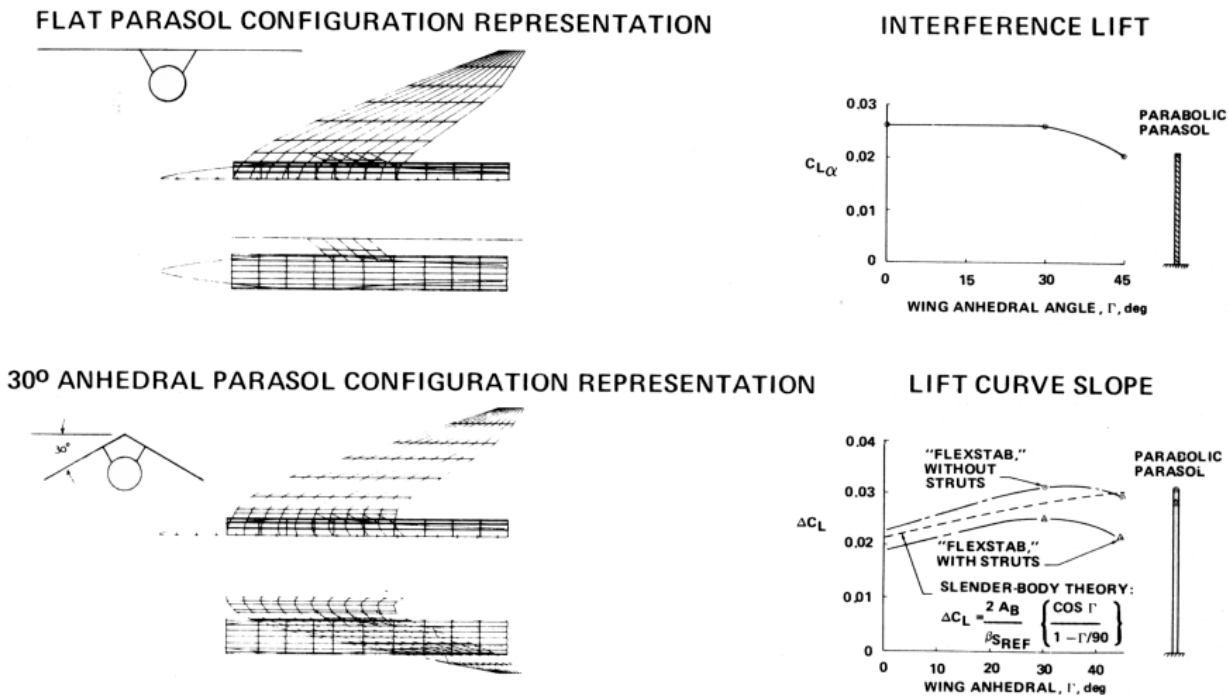

Figure 22. Parasol Wing Lateral Curvature Study Results

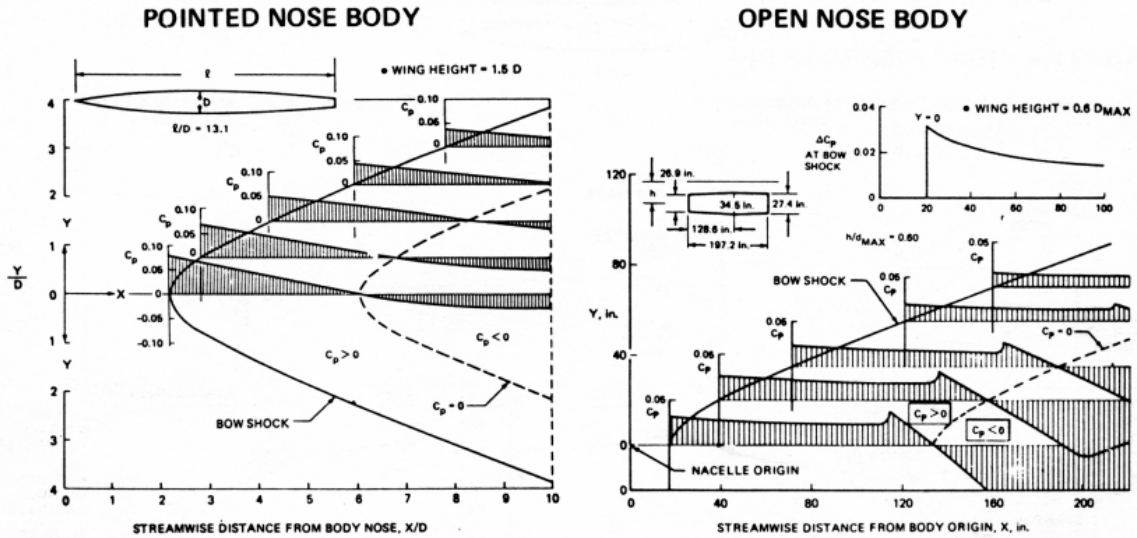

Figure 23. Interference Pressure Distributions

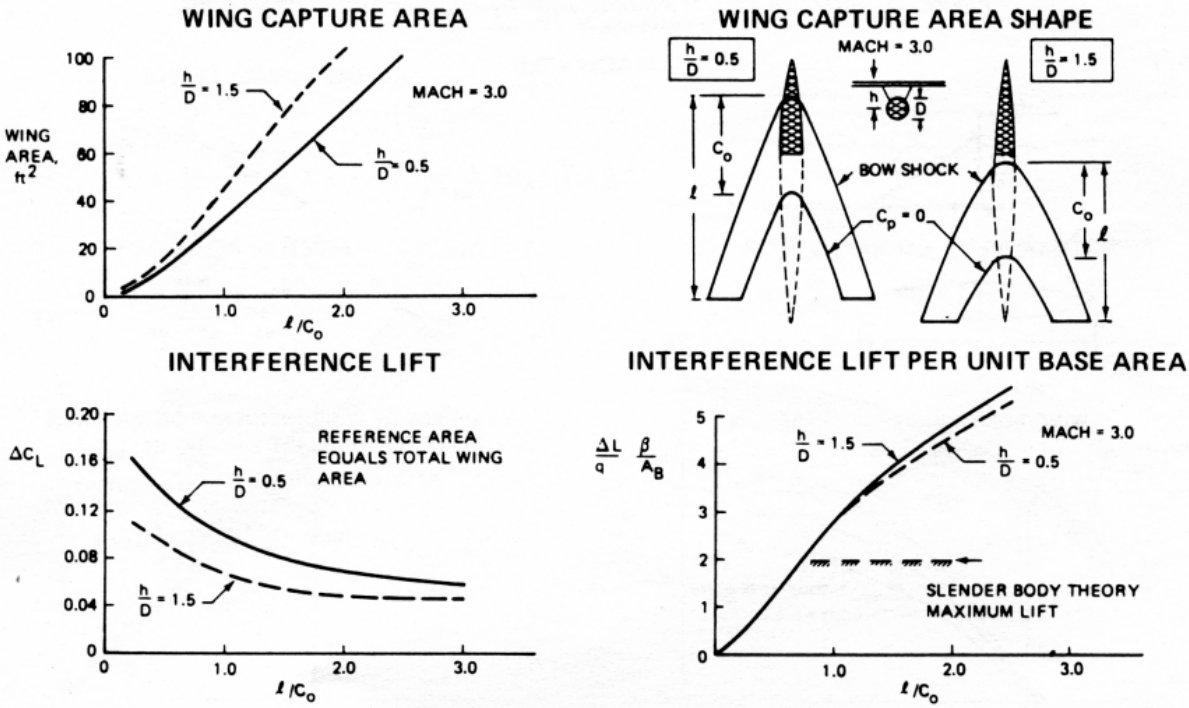

Figure 24. Effect of Wing Planform Length on Interference Lift

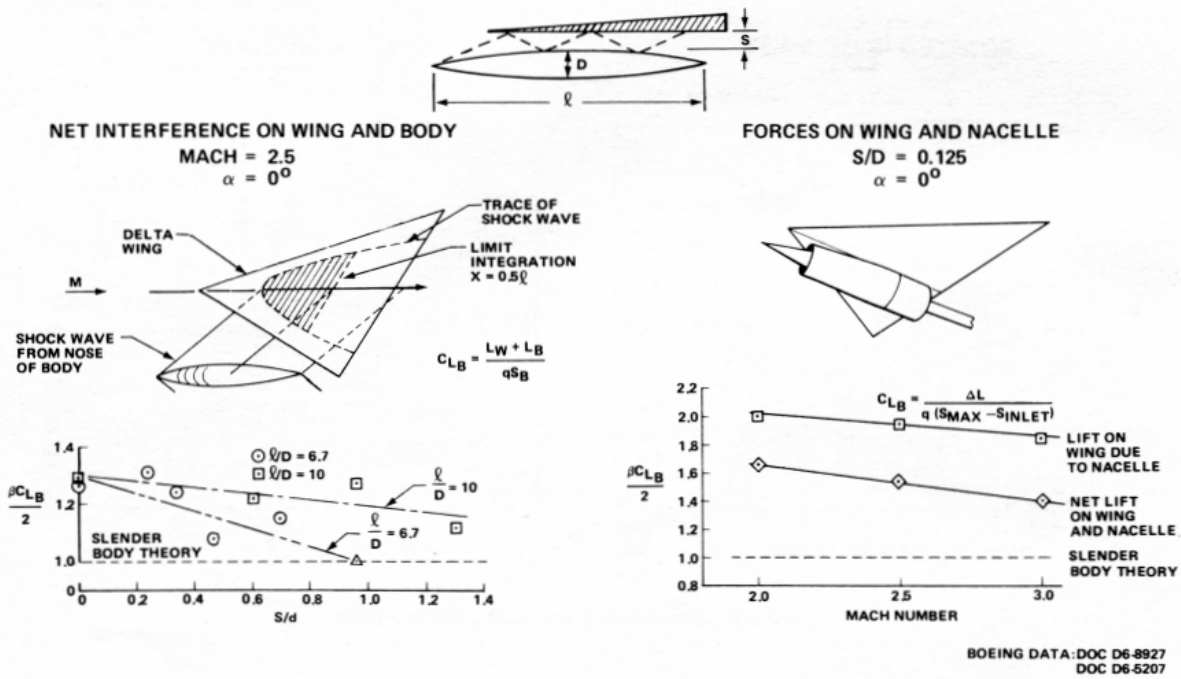

Figure 25. Interference Lift Amplification by Multiple Shock Reflections

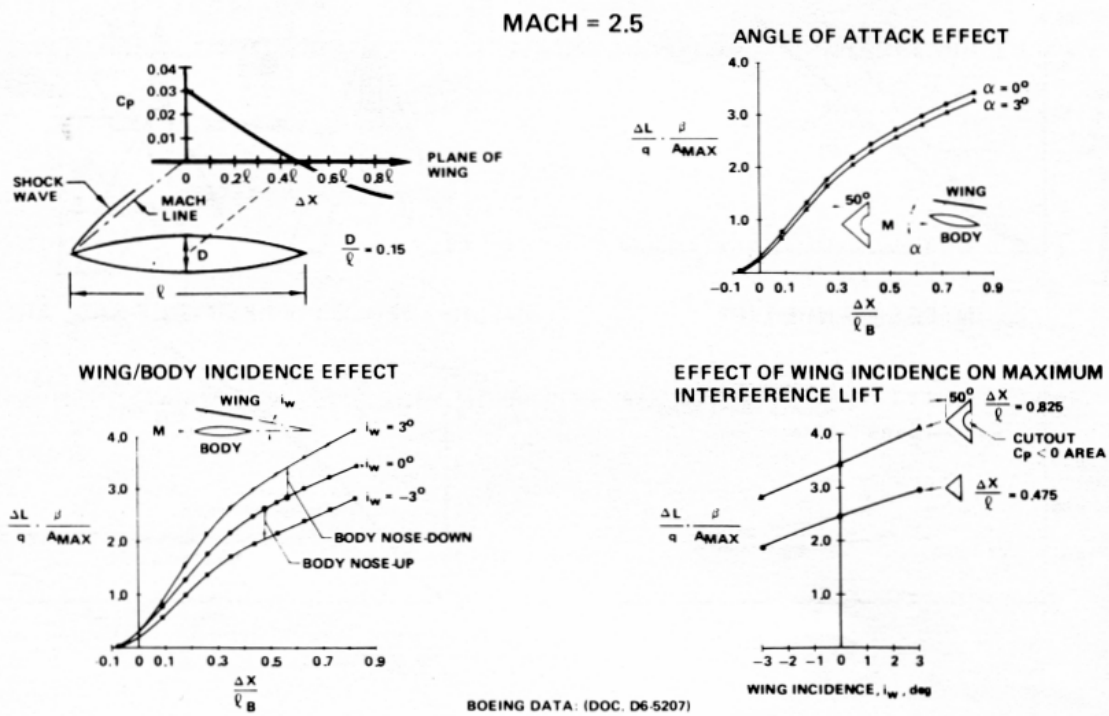

Figure 26. Wing and Body Incidence Effects on Interference Lift

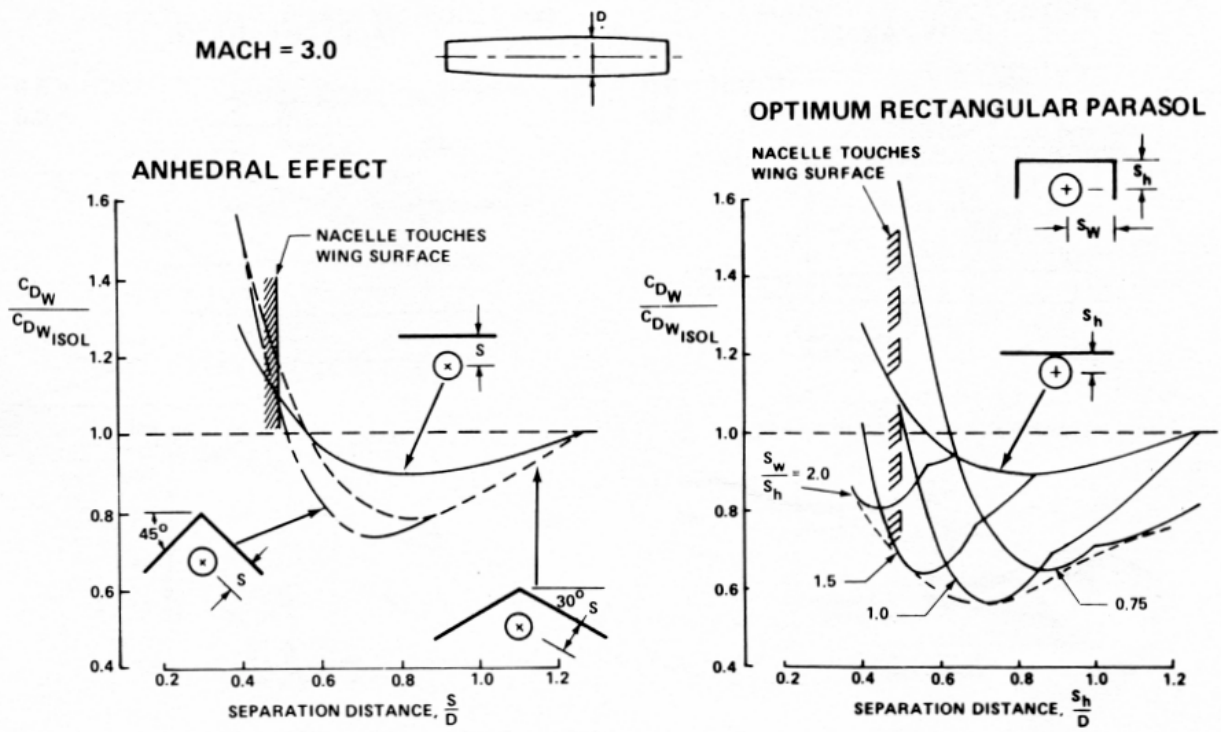

Figure 27. Nacelle Wave Drag Cancellation

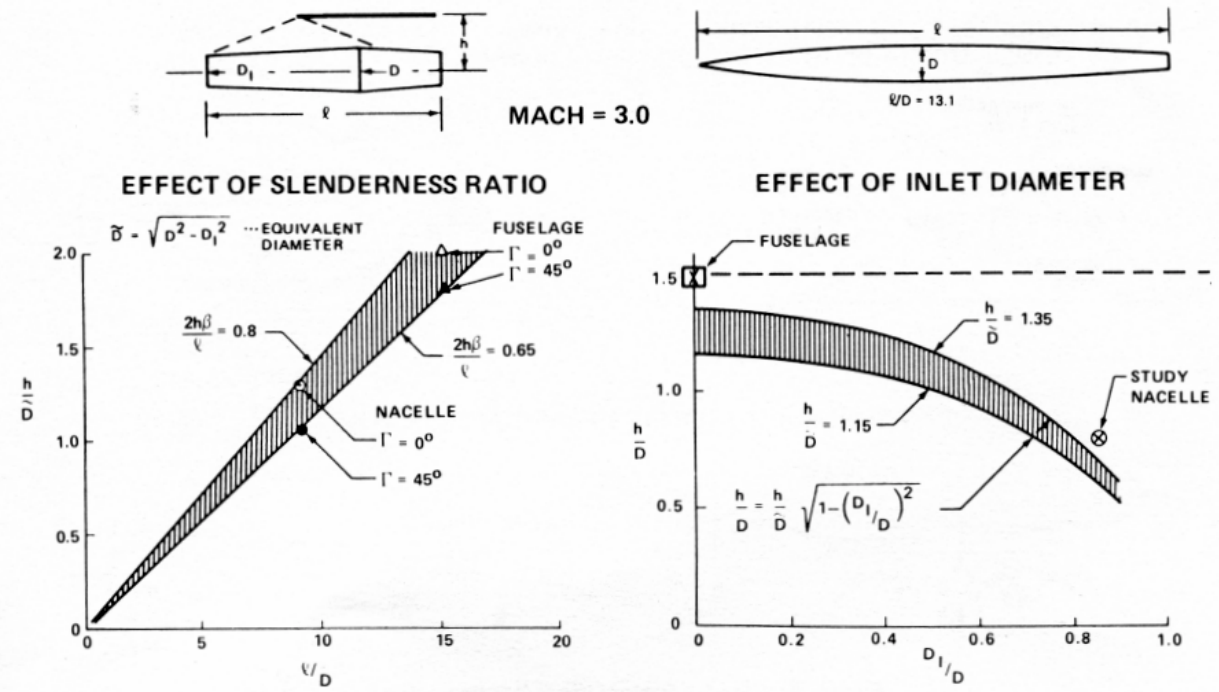

Figure 28. Effects of Body Slenderness and Inlet Diameter on Optimum Separation Distance

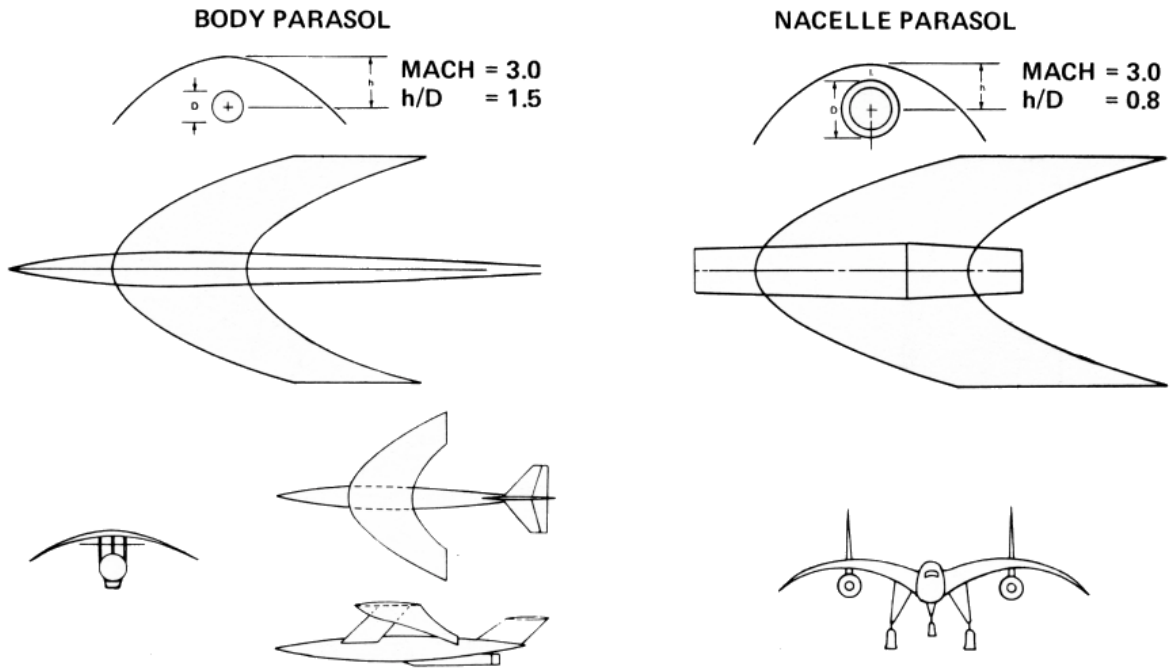

Figure 29. Parasol Wing Configuration Possibilities

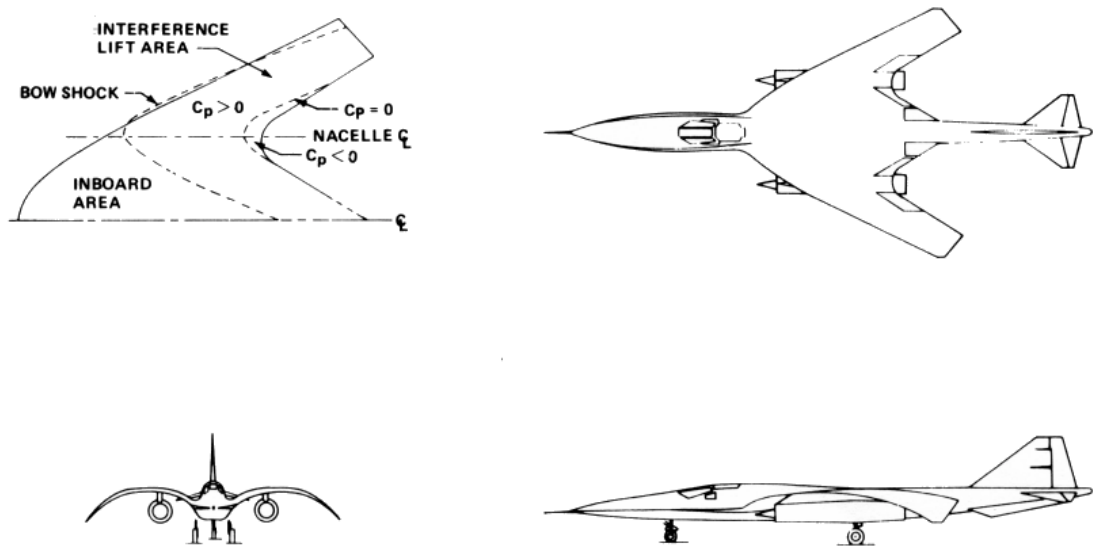

Figure 30. Double-Parasol Wing Configuration

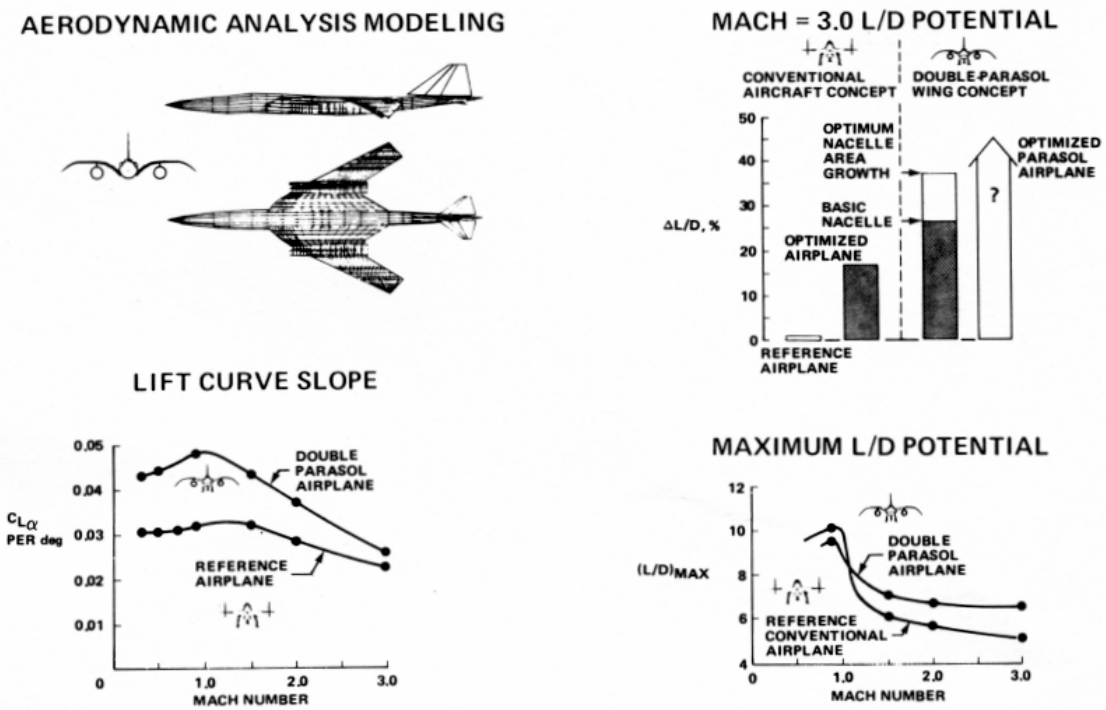

Figure 31. Double-Parasol Wing Configuration Evaluation

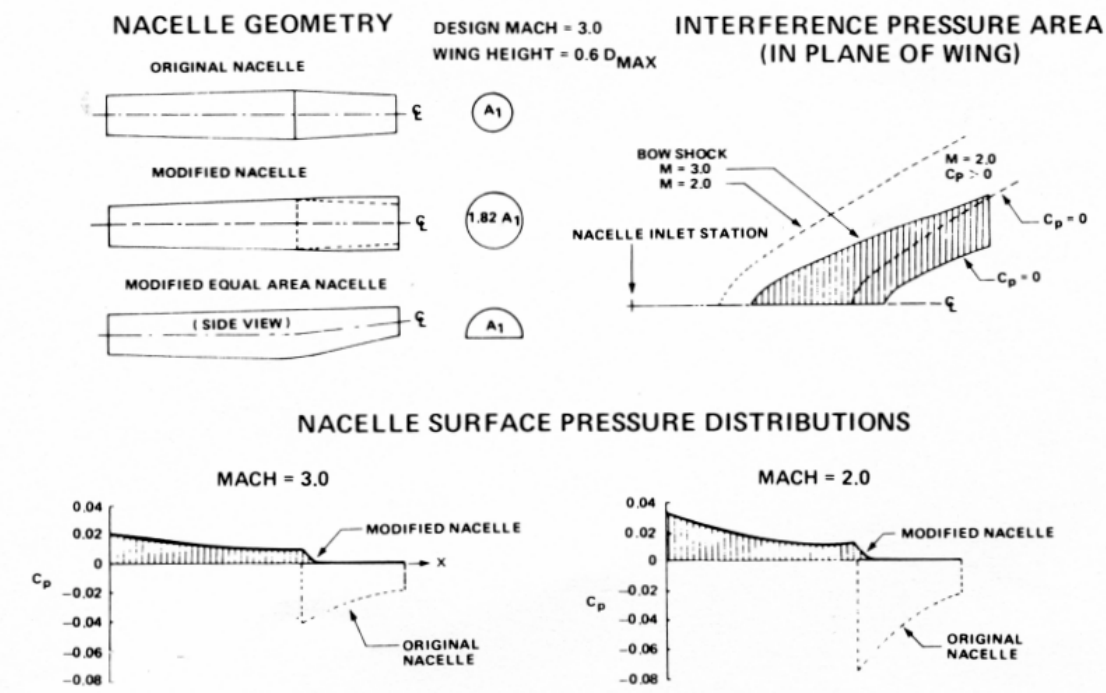

Figure 32. Nacelle Design Modification to Improve Off-Design Interference Lift